ABSTRACT

INA, MARIA. Develop a More Biodegradable/Biocompatible Hemostatic Fabric for Treatment of Bleeding Wounds. (Under the direction of Dr. Samuel M. Hudson and Dr. Wendy E. Krause.)

Hemostatic wound dressings help control traumatic external bleeding by enhancing or accelerating the natural clotting process through various physical reactions. Since the fatal traumatic hemorrhage remains one of the most challenging problems for both military and civilian medicine, efficient hemostatic wound dressings have been in high demand. Currently, several hemostatic dressings have been commercially available for acute hemorrhage, however, they still have some limitations in terms of cytotoxicity, biodegradability, sterilization, and cost performance. Thus, the development of effective biocompatible hemostatic dressings that overcome these limitations has been needed. The goal of this study is to investigate the potential application of *Bombyx mori* silk fibroin fibers as hemostatic wound dressings.

First, the silk fibers were treated with two kinds of neutral salt [calcium nitrate tetra-hydrate ($Ca(NO_3)_2\ 4H_2O$) and calcium chloride ($CaCl_2$)] / alcohol [methanol and ethanol] systems in order to decrystallize their β -sheet crystalline structure and improve the water absorbability and biodegradability. The decrystallization was carried out by controlling the solvent concentration and environment temperature. FTIR and X-ray demonstrated that most effective decrystallization of silk fibers were performed with the treatment in 50% (w/w) $Ca(NO_3)_2\ 4H_2O$/methanol at 65℃, accompanying obvious decrease in the crystal size. Next, the blood clotting ability of the treated silk fibers was investigated by blood coagulation test. Even though any evident blood clot formation on the silk fibers was not confirmed during the test, the blood was separated into two phases and erythrocyte sedimentation was observed at

different rate for each specimen. The silk fibers treated with most severe condition caused slower erythrocyte sedimentation compared with the non-treated silk fibers, suggesting less blood coagulation ability. Previously it has been reported that surface of silk fibroin fibers is hydrophobic and blood proteins interact with the silk fibroin through strong hydrophobic interaction. The obtained results suggest us that the decrease in hydrophobicity of the silk fibers surface due to decrystallization resulted in less interaction with blood proteins. Based on this result, we modified the silk fibers with sodium dodecyl sulfate (SDS) to give hydrophobic portion on the silk fiber surface. The difference in blood coagulation behavior between SDS-modified fibers and non-modified fibers was compared.

Develop a More Biodegradable/Biocompatible Hemostatic Fabric for Treatment of Bleeding Wounds

by
Maria Ina

A thesis submitted to the Graduate Faculty of
North Carolina State University
in partial fulfillment of the
requirements for the degree of
Master of Science

Textile Engineering

Raleigh, North Carolina

2009

APPROVED BY:

Dr. Xiangwu Zhang	Dr. Elizabeth G. Loboa
Dr. Samuel M. Hudson Chair of Advisory Committee	Dr. Wendy E. Krause Co-chair of Advisory Committee

DEDICATION

This work is dedicated to all who support my study at Raleigh.

BIOGRAPHY

Maria Ina was born in Nagano, Japan. She received Bachelor of Science degree in Material Chemistry from Shinshu University, Japan in 2007. During the four years in Shinshu University, her research interest moved toward biomaterials for medical applications. This encouraged her pursue studying biomaterials science at graduate school. She joined College of Textiles, NC State University in Fall of 2007. She has been studying in Textile Engineering program under the direction of Dr. Samuel M. Hudson.

ACKNOWLEDGMENTS

First and foremost, I would like to express my deep and sincere appreciation to my advisor and the chair of Advisory Committee, Dr. Samuel M. Hudson, for giving me the opportunity to work with him and for his continuous guidance and encouragement throughout the entire study. This work would not have been possible without his valuable knowledge and advice. I also wish to offer my sincere thanks to my co-chair of Advisory Committee, Dr. Wendy E. Krause, and other committee members, Dr. Xiangwu Zhang and Dr. Elizabeth G. Loboa for providing oral support and encouragement.

My special appreciations also go to Birgit Andersen, Judy Elson, and Teresa White in College of Textile for training in the use of laboratory facilities. I am grateful to Dr. Nancy Monteiro-Riviere and Ms. Elisha Koivisto in the Veterinary School and Medicine for the blood supply. I am also thankful Mehdi Afshari for microscope operation. Many thanks are also due to Ahmed Mamdouh El-Mekawy, Ahmed Nada, Rupesh Nawalakhe, and Shu Zhang in Textile Engineering, Chemistry, and Science department for their support. I extend my great appreciation all friends at NC State University who spent wonderful time together.

Finally, I have greatly appreciated the professors and all people concerned in Shinshu University for giving me the great opportunity and generous support to study for these two years. I also wish to express my heartfelt appreciation to my family in Japan for their continuous support.

TABLE OF CONTENTS

Page

LIST OF TABLES

LIST OF FIGURES

Page

1. INTRODUCTION

Hemostasis is the physiological process to maintain the integrity of the vascular system by quickly causing the arrest of bleeding from injured blood vessels [1]. It is responsible for minimizing blood loss from the damaged vessels. The fatal traumatic hemorrhage remains one of the most challenging problems for both military and civilian medicine [2]. Currently, it has been reported that uncontrolled hemorrhage cause almost 50% of battlefield deaths [2, 3, 4] and 80% of civilian trauma deaths in the United States [2, 5]. This leads to the need of the development of effective hemostatic dressings that help control traumatic internal and external bleeding, like topical hemostatic wound dressings. The topical hemostatic wound dressings work by enhancing or accelerating the natural clotting process through various physical reactions between the dressings and blood. The ideal topical hemostatic dressings are required to have high hemostatic action, as well as in vivo biodegradability, ease of sterilization, low cost performance, and can be tailored to specific needs [6].

Currently, several hemostatic dressings have been approved by the US Food and Drug Administration (FDA) for acute hemorrhage. The most commonly utilized dressings are the zeolite powder dressing “QuikClot®” and the chitosan wafer dressing “HemCon®”. Zeolite is a hard granule and it promotes rapid clotting by absorbing water molecules quickly from blood, leaving larger platelets and clotting factors behind to concentrate native coagulation elements at the site of vessel bleeding [2, 4, 6]. On the other hand, the chitosan dressing is a fairly rigid wafer that forms a mucoadhesive physical barrier at the site of injury.

HemCon® bandage, which incorporates chitosan as a hemostatic agent into a flexible bandage, becomes sticky when it contacts with blood or other moisture, and adheres to the wound site, sealing it [4]. HemCon® works through ionic interaction by drawing negatively charged red blood cells and platelets to the positively charged bandage, forming a clot and creating an anti-bacterial barrier that protects the wound from infection [4, 6]. However, these commercially available hemostatic dressings have some limitations, such as side effects, a lack of biodegradability, potential for bacterial infections, high cost performance, and hardness of the material [7]. For example, zeolites may cause major thermal injuries came from the exothermic reaction [2, 8-12], remain as foreign bodies in open wounds, and are toxic in the eye or lung [13]. In addition, HemCon® bandages are not large enough or sufficiently flexible to fill large wounds, and work best only on flat surfaces of limited area [6, 13]. A third product, the America Red Cross Fibrin Dressing (human blood fibrinogen) is highly effective but inadequate in availability. It costs $1000 per treatment, which is 100 times over Quikclot® and 10 times over Hemcon® [13].

Recently, it has been researched that the mixture of both these agents demonstrates successful hemostatic properties [2, 8-11]. A granular chitosan dressing Celox®, which is made of zeolite and chitosan, is reported as the newest hemostatic dressing and is non-allergenic, non-exothermic, able to function in a hypothermic environment, and low in cost [2, 4]. It may work by interacting directly with red blood cells and platelets to form a cross-linked barrier clot, independent of native coagulation factors. Overall, recent reviews suggest, however, that each hemostatic dressing has both drawbacks and benefits and that there is no single perfect hemostatic dressings that works for all cases of injures [2, 4, 14]. Therefore,

development of novel hemostatic agents that would overcome these limitations remains an interesting research topic.

Many natural, synthetic and hybrid matrices have been developed to cover wound sites to replace lost tissue functions and support cell growth. For example, aliphatic polyesters, poly(lactic acid) and poly(glycolic acid) are versatile biomaterials, due to their biodegradability and biocompatibility [15-20]. Certain polyurethanes are reported as substrates having biocompatibility and the mechanical and physical properties necessary for a blood-contacting material [21-23]. On the other hand, natural substrates, such as adhesive proteins, have been studied extensively because of their excellent biocompatibility and bioactivity. However, they have high cost difficulties for the establishment of a commercial product.

Chitosan is one of the most attractive biomaterials for various biomedical applications due to its an antibacterial nature and biocompatible and biodegradable properties. It has been reported that chitosan-based hemostatic wound dressings have greater advantages over the other commercially available hemostatic dressings since they have rapid blood coagulation ability (thrombogenicity) as well as non-toxic, antigenecity, bioadhesiveness, and minimal foreign body reactions [24-26]. The chitosan hemostatic dressing, as patented, is relatively expensive (approximately $50-$100 per unit) since it is difficult to produce highly pure medical grade chitosan. Other materials, including collagen, cellulose, or potato starch, have been studied as hemostatic wound dressing materials, but with limited success.

In this study, we pay attention to silk for another biocompatible representative natural polymer. *Bombyx mori* silk fibroin is a natural fibrous protein, mainly consisted of amino acids with small side groups, such as glycine, alanine and serine [13, 15]. In the past few years, there have been increasing interests in the use of silk fibroin in biomedical applications [27, 28] and biotechnological fields [27, 29-32] for the reason of its relatively ease of engineering and excellent mechanical strength in the wet condition [33], biocompatibility for the growth of cells [34], high oxygen and water [35, 36], and drug [37] permeability and resistance against enzymatic degradation [38]. These benefits contribute to its biomedical applications, such as surgical sutures [39], skin treatments [40], enzyme immobilization [41], wound dressing materials [42], substrate for cell culture [34], controlled drug-delivery carriers [43], and scaffolds for tissue engineering [33].

Silk fibroin can be dissolved and regenerated into desired useful forms, such as gel, film, fiber, powder, or non-woven [27, 45-47]. Previous studies on in vitro biodegradation of *Bombyx mori* silk fibroin reported that silk is susceptible to biological degradation by proteolytic enzymes, and the degradation behavior may be highly variable, depending on the structural and morphological features of the polymer (fiber, film, sponge), processing conditions, as well as characteristics of the biological environment, and presence of different mechanical and chemical stresses [48, 49].

In spite of the promising features, however, the biomedical application of fibroin based biomaterials has still not been fully studied. Recently, the study to evaluate the inflammatory of fibroin films revealed that the macrophages, humoral immune component,

adhere to fibroin by filopodia without a complete spreading of the cells [42]. Furthermore, other research group reported the interaction of mouse fibroblast cells with the silk fibroin films. The pure silk fibroin film exhibited as high a cell attachment and growth as collagen [50]. In addition, some studies have been attempted to establish novel biomedical applications of silk fibroin by the modification or combination of silk fibroin with chitosan [44]. For the application for hemostatic wound dressings, the silk fibroin is required the ability of adsorption serum protein. It has previously been reported that the serum proteins, fibrin(ogen), bind to the silk fibroin fibers and films at more hydrophobic β-sheet rich domains through the hydrophobic interaction [42, 51]. Furthermore, the serum protein adsorption onto the silk fibroin fabrics dramatically changed when the conformation of the silk fibroin is rearranged by engineering procedures [52]. These properties suggest that silk fibroin could be used as a useful material for hemostatic wound dressing.

The goal of this research is to evaluate the modification of the silk fiber for its use as a more biodegradable and biocompatible hemostatic wound dressing. In terms of utilization as wound dressings, silk fibroin should be decrystallized partially, to destroy the crystalline β-sheet structure, which should yield improvements of water absorption, protease resorption and blood plasma absorption. It has been known that concentrated aqueous solutions of many inorganic salts, such as halides, bromides, and thiocyanates, readily dissolve silk, in some cases without degradation of the fibroin [53]. For example, aqueous lithium bromide (LiBr) solution [27, 54-55] or aqueous lithium thiocyanate (LiSCN) solution [27, 56, 57] are representative solvents for silk fibroin as well as formic acid. However, we considered that

these solvents are impropriate for modification of silk for use in biomedical application due to their toxicity. In this research, we search for appropriate solvent systems to decrystallize silk fibroin. The resultant changes in its structure were investigated by FTIR, X-ray, and tensile tests. Moreover, blood coagulation tests were carried out and the hemostatic ability of silk fibroin was analyzed.

2. LITERATURE REVIEW

2.1 Chemical composition and primary structure of *Bombyx mori* silk fibroin

Bombyx mori silk fiber is composed of two proteins, fibroin and sericin. Fibroin is extruded from the silkworm gland in the form of filaments embedded in a sericin rubbery coating [42] The fibroin gives the mechanical strength to silk fiber, sericin cements the fibroin filaments together in the silk thread (Figure 2-1). Although sericin is also used in textile processing, *in vivo* studies on silk biocompatibility revealed that the sericin coating is responsible for the immune response and strong immunological reactions take place only when virgin silk is used. Therefore, the sericin is usually removed in a first step by boiling the native silk in alkaline soap water. This process is called degumming. A weight loss of about 22-25% occurs during the degumming process. The degummed silk is considered to be relatively inert [58]. The amino acid compositions of the silk fibroin are shown in Table 2-1 [59]. *Bombyx mori* silk fibroin contains a high proportion of three α -amino acids, glycine (G; Gly), alanine (A; Ala), and serine (S; Ser), in the approximate molar ratio of 3:2:1, respectively [27]. In terms of the structure, native silk fibroin is originally present as an extensive anti-parallel β -sheet crystalline structure (silk II, Figure 2-2, 2-3) with highly repeated Gly-Ala-Ser sequence, induced by the mechanical stresses during the cocoon spinning [60, 61]. These amino acids with relatively small side groups make it possible for the molecular chains to pack closely. These extended zig-zag chains interact each other by hydrogen bonds (Figure 2-4) and form the β -sheet structure with a very high fiber

crystallinity of around 70%. Between the β-sheets, only van der Waals forces work. The crystalline structure is interspersed by a more flexible amorphous domain, which consists of the more bulky amino acids, such as aspartic acid [62], giving the silk the characteristic of a block co-polymer structure. This characteristic structural configuration gives silk fibroin its unique mechanical properties, including high strength and flexibility (Table 2-2).

Molecular weight data of silk fibroin have been somewhat inconclusive in that a variety of results have been obtained by the use of different measurements; 400kDa by ultracentrifugation, 370kDa by sedimentation analysis, and by light scattering, values of 435kDa [63]. The reason for this is that different molecular weight averages are being measured and perhaps different degrees of aggregation. Cantor et al. [64] reported that Gly and Ala rich polypeptides behave as if they are much larger than their true sizes by electrophoresis measurement. For these reasons, it has been difficult to measure its exact molecular weight. However, it is generally believed that silk fibroin has a molecular weight of approximately 400kDa; heavy chain of 350kDa, light chain of 26kDa, and P25 of 30kDa [65] from electrophoresis and gene sequencing studies.

Table 2-1 Amino acid composition of *B*ombyx *mori* silk proteins in percentage of total amino acids (Cp, chymotrypsin precipitate; Cs, chymotrypsin soluble). [59]

	Whole fibroin	C_p fraction	C_s fraction	Sericin
A (alanine)	29.3	32.89	22.16	5.2
D (aspartic acid)	1.3	0.56	3.87	14.6
R (arginine)	0.5	0.18	1.29	2.8
C (cystine); half	0.2	0.00	0.00	0.3
E (glutamic acid)	1.0	0.43	2.58	7.9
G (glycine)	44.5	48.00	36.85	13.5
H (histidine)	0.2	0.06	0.50	1.0
I (isoleucine)	0.7	0.13	1.80	0.6
L (leucine)	0.5	0.00	1.29	0.8
K (lysine)	0.3	0.20	0.77	4.3
M (methionine)	0.1	0.00	0.00	0.1
F (phenylalanine)	0.6	0.13	1.54	0.5
P (proline)	0.3	0.00	1.03	0.5
S (serine)	12.1	14.97	6.96	33.1
T (threonine)	0.9	0.36	2.32	8.3
W (tryptophan)	0.2	0.00	0.00	0.3
Y (tyrosine)	5.2	1.40	10.80	3.1
V (valine)	2.2	0.64	5.67	3.1

Table 2-2 *Bombyx mori* silk as a raw material. [27]

Produced by	Fiaçào de Seda Bratac S.A., Brazil
Size deviation	0.69denier
Evenness	3 stripes
Cleanness	98.60%
Neatness	97.55%
Maximum deviation	1.8denier
Tenacity	4.16g/den
Elongation	21.2%

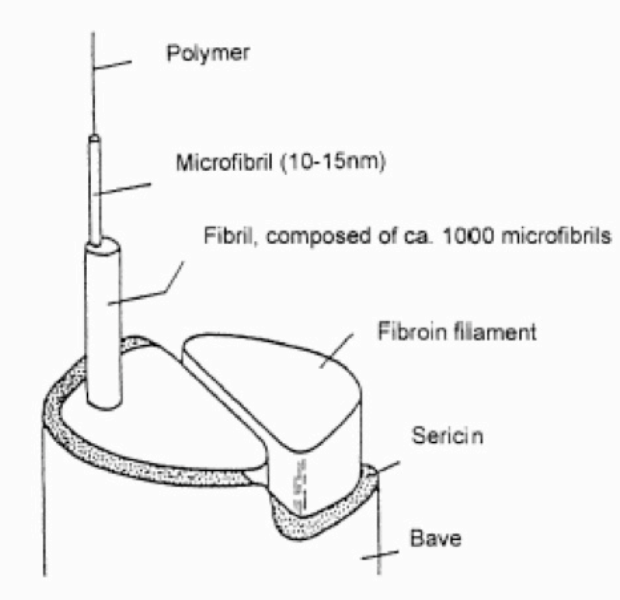

Figure 2-1 Schematic of silk thread. [102]

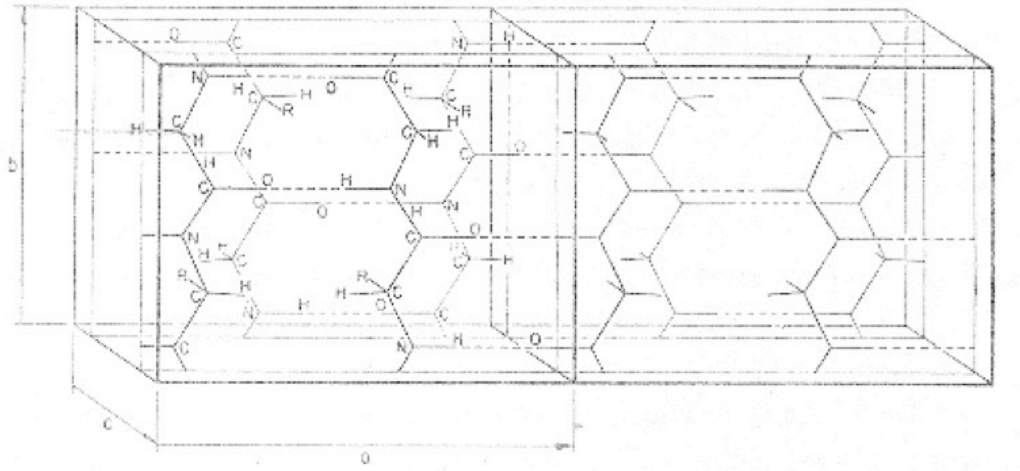

Figure 2-2 Crystalline unit cell of silk II proposed by Marsh et al. [59]

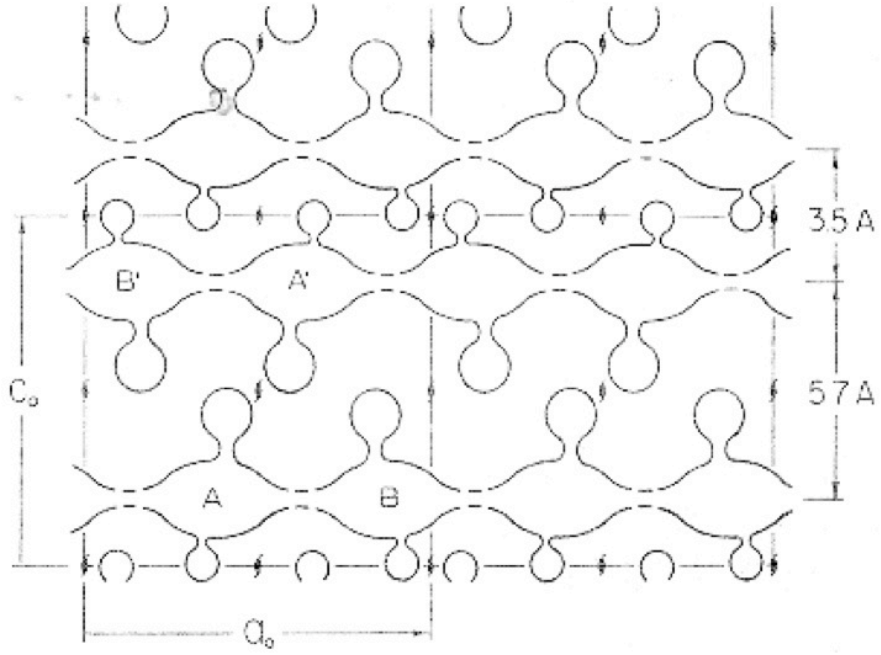

Figure 2-3 Projection of intersheet distribution along fiber axis. [59]

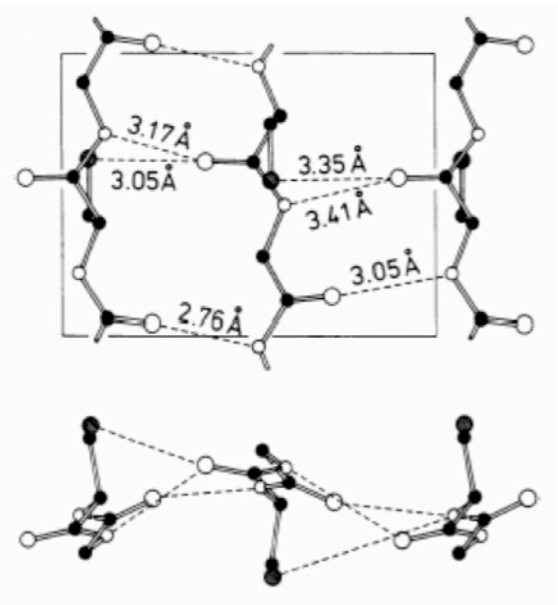

Figure 2-4 Hydrogen bonding structure of serine residues with neighboring chain in silk II structure. [103]

2.2 Crystalline structure of native silk fiber (Silk II)

A number of studies have been done on the crystal structure of silk fibroin (silk II) with X-ray diffraction [66]. These studies proposed that silk II has an orthogonal unit cell (a= 9.38Å; hydrogen bonding direction, b=9.49Å; fiber axis, c=6.98Å; inter sheet distance) and described silk II as having an anti-parallel chain pleated β -sheet structure (Figure 2-5). They assumed that the crystalline unit cell contains only Gly, Ala, and Ser residues. Larger amino acids, such as Tyr (tyrosine; T) and Leu (leucine; L) are located in amorphous regions [67]. Four chains (eight amino acid residues) are fitted in the unit cell along the *b*-axis (fiber axis) and two pleated sheets are accommodated in it (Figure 2-2). Spacing of pleated sheets along the *c*-axis was obtained from the intensities of equatorial reflections (*00l*). The distance between adjacent pleated sheets has been reported alternately as 3.5Å and 5.7Å (Figure 2-3). Therefore, two pleated sheets solely of Gly residues may pack together at a distance of 3.5Å, whereas sheets containing Ala and Ser may pack together at a distance of 5.7Å. From the Scherrer equation with the half-width of the equatorial reflections, the lateral dimensions of the crystallites are about 59Å to the *a*-axis and about 22Å to the *c*-axis. About five pleated sheets each with 12 chains are accommodated in a crystallite.

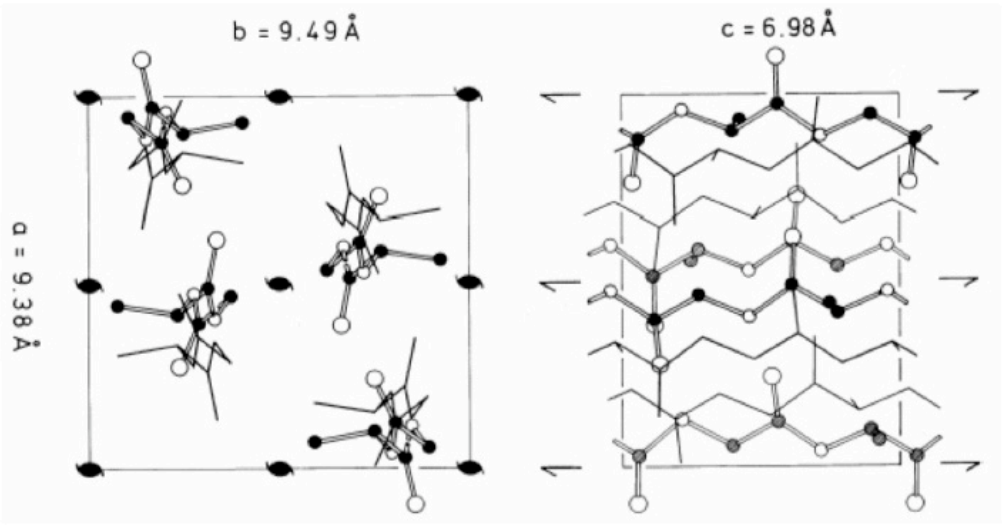

Figure 2-5 Refined unit cell structure of silk II proposed by Takahashi et al. [103]

2.3 Solvent/ Decrystallizing agents for silk fibroin

In order to regenerate the silk fibroin into various desired forms such as like gel, film, fiber, powder, or non-woven, a dissolution process is necessary to destroy the crystalline β -sheet structure and solubilize the fibroin [27, 68]. Silk fibers consist of highly ordered arrangements of fibroin chains linked together by intermolecular hydrogen bonds [68, 69]. Freddi et al. investigated the effect of organic reagents with a dehydration action, such as methanol, on the re-crystallization of silk fibroin film by observing the change from random coil structure (silk I, Figure 2-6) to crystalline β -sheet conformation (silk II) [32, 68, 70]. On the other hand, in order to dissolve silk fiber effectively, swelling of the compact fibrous

structure and breaking of the hydrogen bond network are required, resulting in complete dispersion of the individual fibroin molecules. An ideal solvent of silk fibroin should be capable of penetrating into the fiber and dissolving it without inducing adverse reactions, such as depolymerization, derivatization, etc [68].

The most common solvents used for silk are formic acid and concentrated aqueous lithium salt solutions and neutral salt-water alcohol systems. 9M aqueous lithium bromide (LiBr)[71,72] or 9M aqueous lithium thiocyanate (LiSCN) solution [57, 68, 73, 74] are usually chosen because its solution is neutral and active at room temperature and unlikely to cause peptide bond hydrolysis [68]. Other concentrated salt solutions, such as NaSCN and $ZnCl_2$ solutions can also be used for the dissolution of silk [68, 75, 76]. In addition, neutral salt-water-alcohol systems have also been reported to be effective in dissolving silk. Ajisawa et al. reported the calcium chloride-ethanol system (molar ratio of $CaCl_2$: H_2O: EtOH=1:8:2) [68,77-80]. As shown in Table 2-3(a,b), the dissolution of silk fibroin was greatly improved by adding ethanol into calcium chloride aqueous solution at that molar ratio. Furthermore, Mathur at al. [32, 68, 70, 81] recently reported on the discovery a novel salt system as a solvent of silk fibroin, composed of calcium nitrate hydrate and methanol, $Ca(NO_3)_2$ $4H_2O$/MeOH system (molar ratio of Ca:H_2O:MeOH=1:4:2), as well as on the properties of regenerated silk fibroin films and fibers. In any case, these salts (lithium or calcium) should be removed by dialysis since these fibroin solutions contain considerable amounts of salt [82].

In general, it is known that the regenerated fibroin materials show poor tensile properties and brittleness compared with the original silk fiber [27, 45-47]. However, Ha et al.

reported that these problems can be technically solved by improving a fiber processing method [27] (Table 2-4(a-c), Figure 2-7).

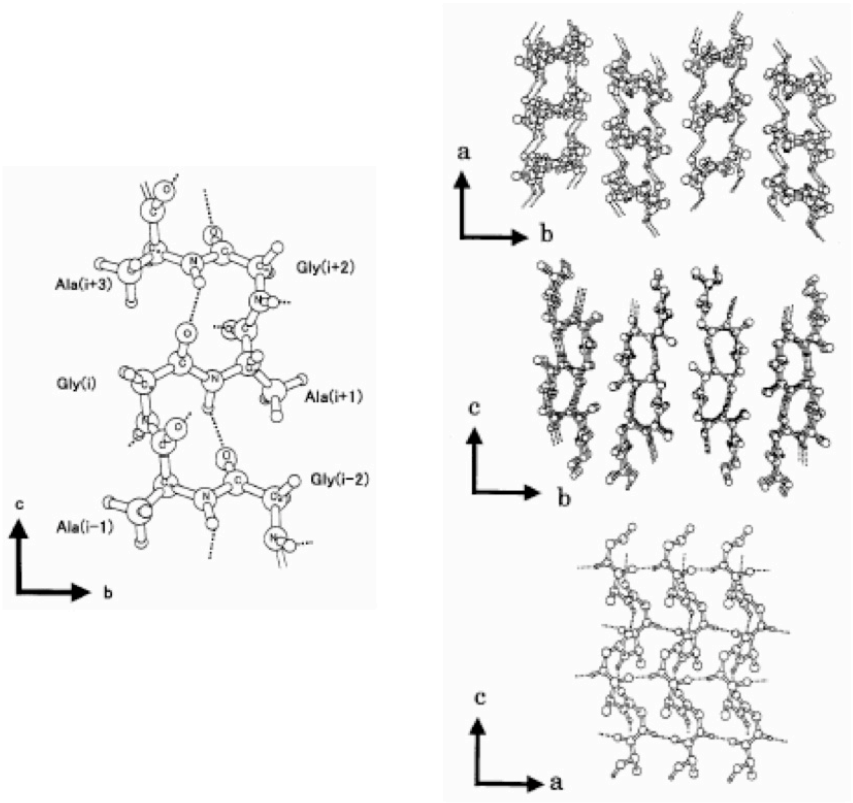

Figure 2-6 Repeated β-turn model of silk I proposed by Asakura et al. [104]

Table 2-3 (a) Solubility (%) of fibroin at 20~30℃. [77]

dsissolved condition		solution	
temperature (%)	hours (hr)	*S_1	**S_2
20	240	0	55.8
	720	0	97.3
30	240	0	88.0
	720	0	100.0

* S_1…Calcium chloride:water=1:8 mol solution.
**S_2…Calcium chloride:water:ethanol=1:8:2 mol solution.

Table 2-3 (b) Solubility (%) of fibroin at 40~60℃. [77]

dissolution	solution		rate
temperature (℃)	*S_1	**S_2	**S_2/*S_1
40	0.7	14.7	21
50	1.3	47.3	36
55	2.7	100.0	37
60	3.3	100.0	30

* S_1…Calcium chloride:water=1:8 mol solution.
**S_2…Calcium chloride:water:ethanol=1:8:2 mol solution.

Table 2-4 (a) Measured fineness of regenerated fibroin fiber samples (unit = denier). [27]

	Original silk fiber	As-spun fiber from formic acid dope	Drawn fiber from formic acid dope	As-spun fiber from TFA dope	Drawn fiber from TFA dope
1	0.719	43.40	~~3.65~~	8.694	~~6.263~~
2	~~1.408~~	26.78	11.11	~~3.359~~	3.102
3	1.354	29.84	16.98	10.360	6.178
4	0.832	28.28	~~22.18~~	5.310	6.185
5	~~0.691~~	~~22.80~~	9.97	10.031	2.903
6	0.821	31.05	15.43	3.986	3.220
7	0.902	~~47.06~~	9.50	~~20.495~~	5.552
8	0.802	36.20	10.81	10.243	~~1.672~~
9	0.904	25.74	11.16	5.881	1.839
10	1.060	30.22	10.14	10.221	5.905
Average	**0.949**	**32.14**	**12.09**	**8.858**	**4.282**

Table 2-4 (b) Tensile properties of regenerated fibroin fibers (Average deniers obtained from VIBROMAT® (Table 2-4 (a) were used as inputs). [27]

Sample	Original silk fiber			As-spun fiber from formic acid dope			Drawn fiber from formic acid dope			As-spun fiber from TFA dope			Drawn fiber from TFA dope		
Tensile property	% strain at break	Modulus	Tenacity	% strain at break	Modulus	Tenacity	% strain at break	Modulus	Tenacity	% strain at break	Modulus	Tenacity	% strain at break	Modulus	Tenacity
1	24.01	95.09	5.50	2.35	254.41	1.98	26.54	379.06	9.85	1.19	168.32	1.82	11.63	418.84	6.99
2	21.00	112.99	4.33	2.39	273.03	2.14	13.20	246.94	7.10	1.97	343.25	4.60	10.04	413.58	8.32
3	15.10	101.87	4.67	2.29	292.02	2.47	39.95	305.86	8.98	1.06	323.73	2.93	16.44	260.16	7.54
4	35.81	82.00	5.63	2.66	279.59	2.73	38.29	261.52	8.29	2.11	162.88	2.46	13.14	296.29	7.48
5	27.23	92.33	5.22	1.90	237.27	1.16	16.97	302.99	6.81	1.10	296.14	2.84	19.29	485.59	6.73
6	24.70	90.89	4.50	3.30	300.61	3.97	37.95	405.26	10.17	0.66	255.64	1.34	19.68	344.11	7.23
7	25.89	121.64	5.97	2.39	238.70	2.62	37.75	329.45	9.36	1.86	111.20	0.71	15.05	284.36	7.30
8	26.41	83.49	5.27	2.35	214.64	1.89	18.82	317.04	6.73	1.21	276.58	2.94	17.03	412.95	8.43
9	24.43	122.44	5.24	3.08	251.55	2.96	45.93	317.61	10.19	0.78	261.84	1.79	27.35	344.14	10.11
10	34.24	103.45	6.15	2.67	290.77	3.63	17.99	290.75	7.82				31.55	362.01	10.29
Average	25.89	100.62	**5.25**	2.54	263.26	**2.56**	29.34	315.65	**8.53**	1.33	244.40	**2.38**	18.12	362.20	**8.04**

Table 2-4 (c) Tensile data of regenerated fibroin fibers using traditional wet drawing method. [27]

Draw ratio	3x	4x	5x
Fineness (den)		41	
Tenacity (g/den)	1.08	2.20	Expecting increase
Elongation (%)	30.8	14.2	Expecting decrease

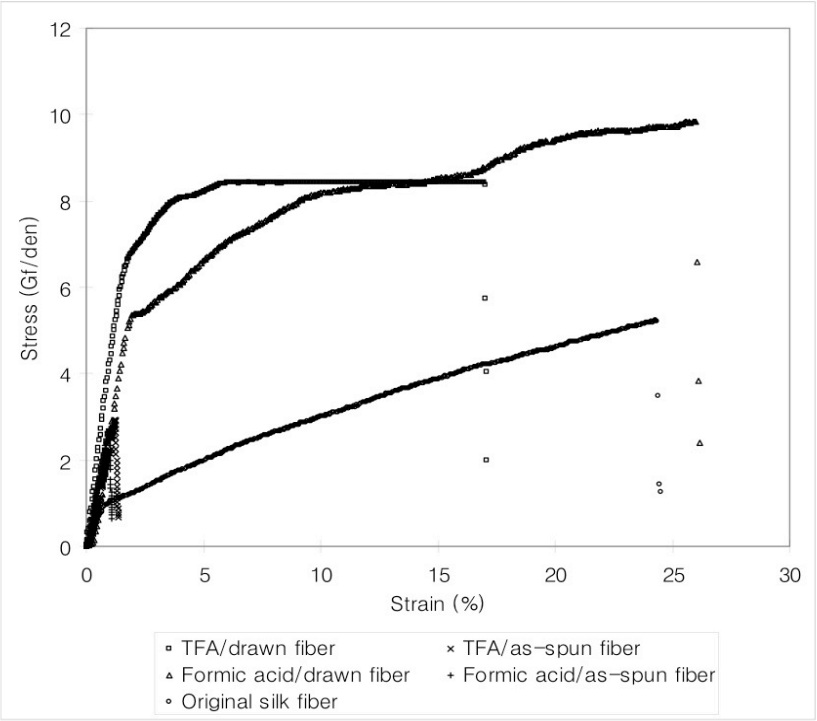

Figure 2-7 Stress-strain curve of regenerated fibroin fibers. [27]

2.4 Dissolution of silk fibroin in $Ca(NO_3)_2$ $4H_2O$/MeOH

Ha et al. examined the effect of water for the dissolution of silk fibroin in calcium nitrate/ methanol system, Ca $(NO_3)_2$ nH_2O (n is the hydration number), defining amounts of water added to anhydrous calcium nitrate [70]. Figure 2-8 [70] shows the difference in dissolution of silk fibroin in the calcium nitrate/methanol solvent system with various hydration numbers with concentrations range of calcium nitrate/methanol between 40% (w/w) and 95% (w/w). The fibroin concentrations were varied as 5%, 10%, 15%, and 20%

(w/v). They revealed that the anhydrous and mono-hydrate calcium nitrate/methanol solutions could not dissolve fibroin at all, di-hydrate calcium nitrate/methanol solutions only swell the fibroin, and the calcium nitrate/methanol solutions with hydration numbers over three dissolved the silk fibroin [82]. Furthermore, a 75% (w/w) tetra-hydrate calcium nitrate/methanol solution [$Ca(NO_3)_2$ $4H_2O$/ MeOH] was the optimum concentration that can dissolve the silk fibroin [82].

Figure 2-9 [70] shows the phase diagram for the dissolution of silk fibroin in the $Ca(NO_3)_2$ nH_2O/MeOH system with various solvent concentration ranges. These results indicated that at least three water molecules per one calcium ion are needed to begin dissolution of silk fibroin. The most critical factors for the fibroin dissolution are the molar ratios of calcium nitrate, water, and methanol, moreover, the optimum ratio is 1:4:2 as shown in Figure 2-10. However, the mechanism for the dissolution of silk fibroin is still uncertain.

In the related system, Aoki [83] proposed that the oxygen atoms of the carbonyl groups in the amide bonds of Nylon 6 make coordination bonds with calcium ions in $CaCl_2$ $2H_2O$/MeOH system (Figure 2-11 [83,84]). Just like the case of Nylon 6 in $CaCl_2$ $2H_2O$/MeOH system, Ha et al. considered that the oxygen atoms of the carbonyl groups in the peptide bonds of fibroin also seem to make coordination bonds with calcium ions in $Ca(NO_3)_2$ $4H_2O$/MeOH [70, 82]. However, the dissolution mechanisms for both cases would not be the same since fibroin-calcium nitrate/methanol system requires four water molecules per one calcium ion for the complete dissolution, as mentioned above. For this reason, they [70, 82] assumed that the water molecules act either as a swelling agent for the silk fibroin or as components of the coordination bonds. They proposed the complex structure of the solvent

and fibroin shown in Figure 2-12 [82]. It is considered that three water molecules per calcium ion play an important role in the coordination of carbonyl groups in peptide bonds of fibroin and the calcium ions.

The dissolution process is a physical phenomenon. Dissolution requires the proper ratios of calcium ions and ligands, which is also dependent on the nature of the calcium counter ion. If the binding of the solvent ligands and counter ions to the calcium are too strong, dissolution will not occur. In this case, the combination of nitrate, water, and methanol gives a correct balance [70].

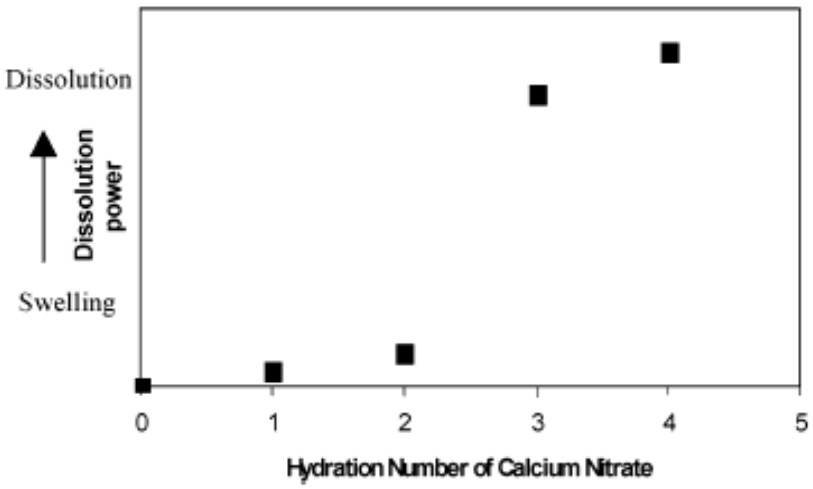

Figure 2-8 Effect of hydration number in the $Ca(NO_3)_2$-MeOH-H_2O solvent system for the dissolution of silk fibroin. [70]

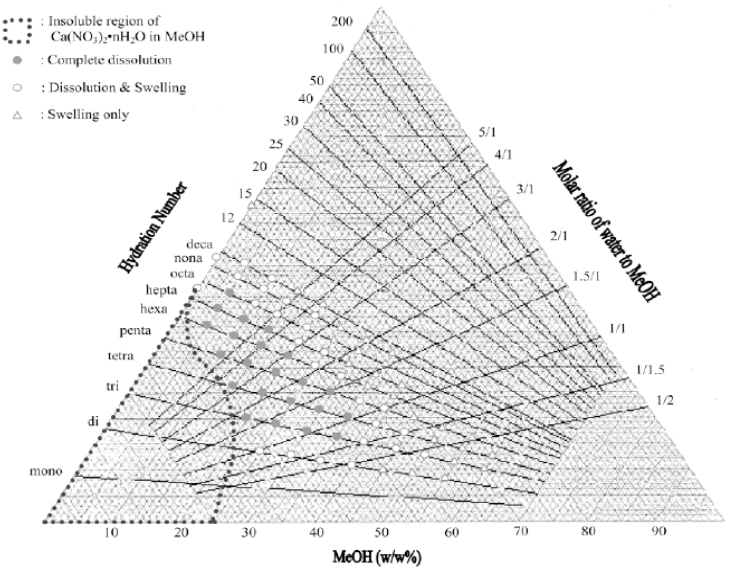

Figure 2-9 Dissolution phase diagram for fibroin solution in various solvent concentration ranges of $Ca(NO_3)_2$ nH_2O-MeOH. A 10% w/v fibroin concentration was used. The insoluble region of calcium nitrate is shown by a dotted line in the region nearest pure calcium nitrate. [70]

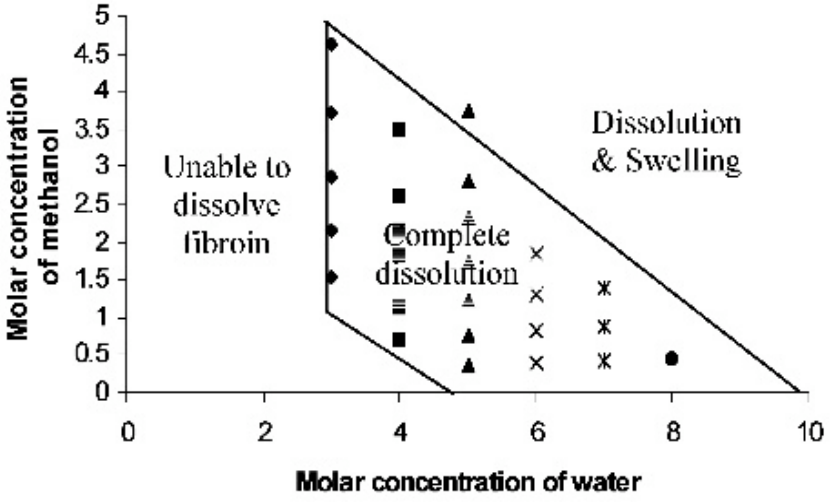

Figure 2-10 Molar ratio of MeOH to H_2O required for dissolution of silk fibroin when [Ca^{2+}] is 1 mol. [70]

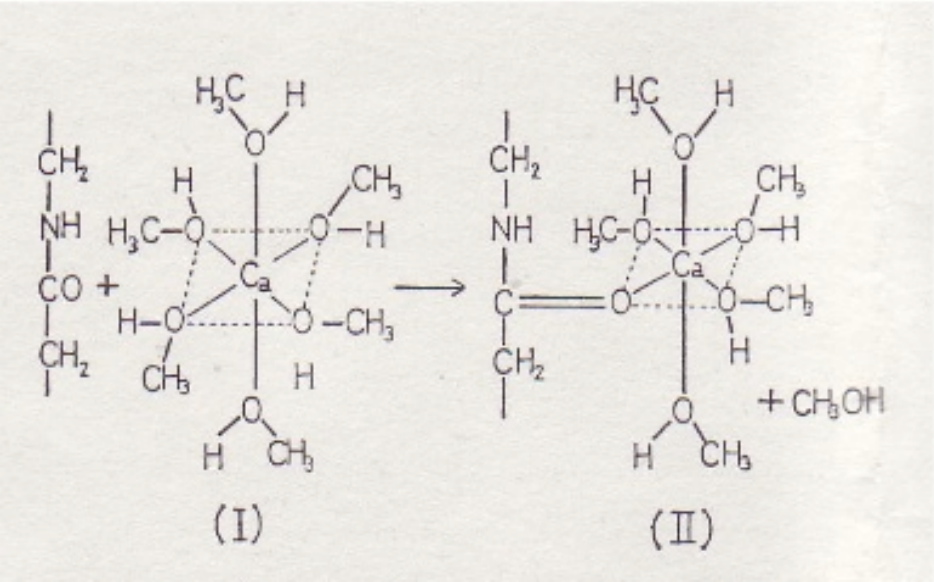

Figure 2-11 Dissolution mechanism of Nylon 6 in $CaCl_2$-methanol system, as proposed by Aoki. [84]

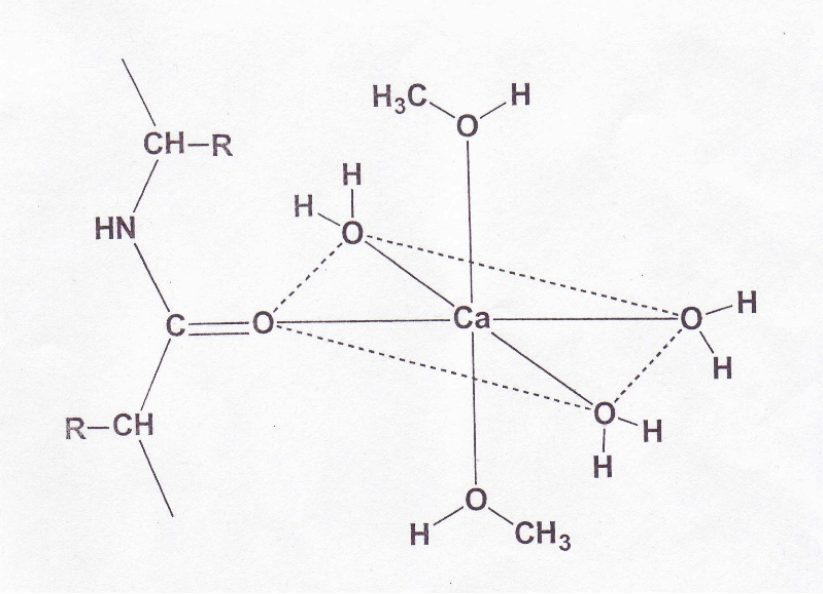

Figure 2-12 Proposed complex between a calcium ion and a peptide bond of fibroin. [82]

2.5 Protease enzymes that degrade silk

In vitro biodegradation of *Bombyx mori* silk fibroin has revealed that silk fibroin is susceptible to enzymatic degradation and it depends on the structure and morphology of the silk polymer [36, 56, 57]. Arai et al. reported that when water-insoluble silk films treated with methanol were exposed to different proteolytic enzymes, such as collagenase, α-chymotrypsin, or protease, the cleavage of the fibroin chains and formation of a range of soluble peptides were caused. With increasing contact time with enzymes, the total content of glycine, alanine, and serine in the film gradually increased, on the other hand, those of tyrosine, valine, and other amino acids with polar and bulky side groups accordingly decreased. As mentioned above, it is known that the silk fibroin has crystalline regions which consisted of three simple amino acids with small side groups, glycine, alanine, and serine, and the amorphous regions which are highly enriched in amino acids with bulky and polar side groups [56]. Therefore, the results indicated that the enzyme molecules could penetrate into the swollen amorphous regions of the silk fibroin chain more easily than crystalline regions or highly dense regions, resulting in cleavage of the sensitive peptide bonds distributed along the amorphous regions and releasing free soluble peptides. Also, they found that silk films exhibited a noticeable decrease of the weight and degree of polymerization, compared to silk fiber. Unlike fiber, silk films are isotropic in nature, thus the amorphous phase is more likely to swell. For this reason, films are readily degraded by protease, while fibers are more resistant to proteolytic attack [36, 56].

In addition, the extent of biodegradation of silk fibroin also may depend on the kind of enzyme used, as well as on the structure and morphology of the substrate [56]. The

protease from *Streptomyces griseus* (*S.griseus*) was considered to be more aggressive to silk films than other enzymes, resulting in local loss of strength and elongation, randomly distributed along the fibers. It seems that enzymes are likely to cause localized degradation along the fiber axis, corresponding to more accessible sites where proteolysis could occur due to closer enzyme-fiber interaction.

2.6 Mechanism of blood coagulation (Hemostasis)

The blood coagulation (hemostasis) mechanism is still under investigation because of the complexcity of the hemostatic-thrombotic system [16]. Hemker et al. introduced the first law of hemostasis and thrombosis: increasing thrombin formation causes more thrombosis but less bleeding, and decreasing thrombin formation causes more bleeding but less thrombosis [16]. Hemostasis includes the complex interaction between vessels, platelets, coagulation factors, coagulation inhibitors, and fibrinolytic proteins to maintain the blood within the vascular compartment in a fluid state. When a vessel is damaged, the hemostasis proceeds by the following stepwise mechanisms. First of all, vasoconstriction occurs to reduce the diameter of the vessel at the sites of injury and instantly minimize blood loss. Following that, platelets adhere to collagen in the exposed walls of the damaged vessel and promote the formation of a soft aggregate platelet plug. A complex cascade of reactions and factors involves to stabilize the soft clot and maintain the vascoconstriction. A factor activates another factor in sequence. It has been studied that at least 12 plasma proteins interact in a series of enzymatic and cofactor reactions leading to blood clotting as shown in Figure 2-13, 14 [1]. Especially, thrombin is the enzyme that plays an important role in

formation of clots. Fibrinogen, a soluble glycoprotein, is converted to fibrin in the coagulation cascade by the thrombin. The fibrin, a fibrous protein, initially forms a loose mesh and then is crosslinked by Factor XIII to form a dense mesh that act as a hemostatic plug or clot over the wound site in the presence of calcium ions. In consequence, platelets and red blood cells become caught in this covalently crosslinked mesh of fibrin fibers, finally the arrest of bleeding is accomplished. Finally, hemostasis is completed by fibrinolysis that removes the hemostatic plug and improves blood flow through the damaged vessel after the stoppage of bleeding and healing process [1].

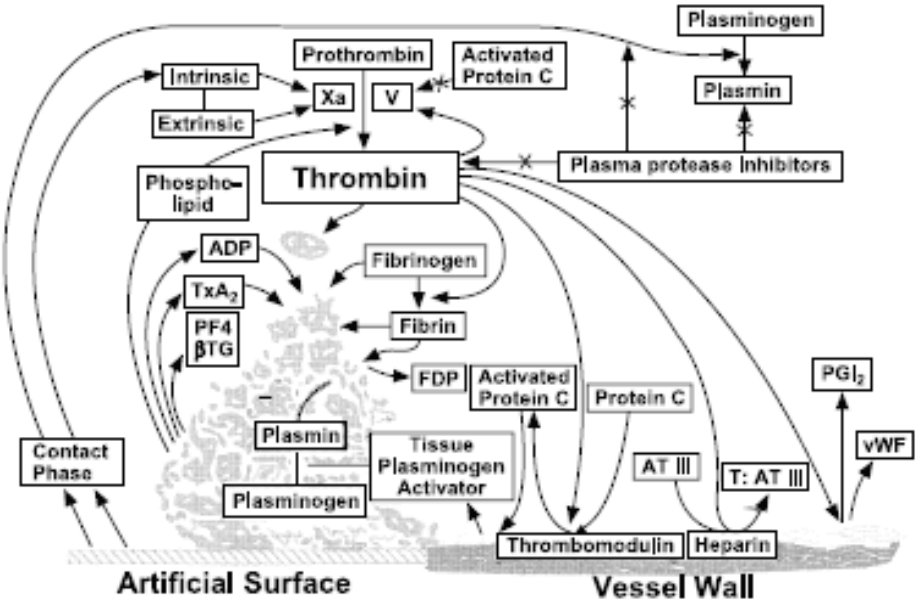

Figure 2-13 Integrated hemostatic reactions between a foreign surface and platelets, coagulation factors, the vessel endothelium, and the fibrinolytic system. [1]

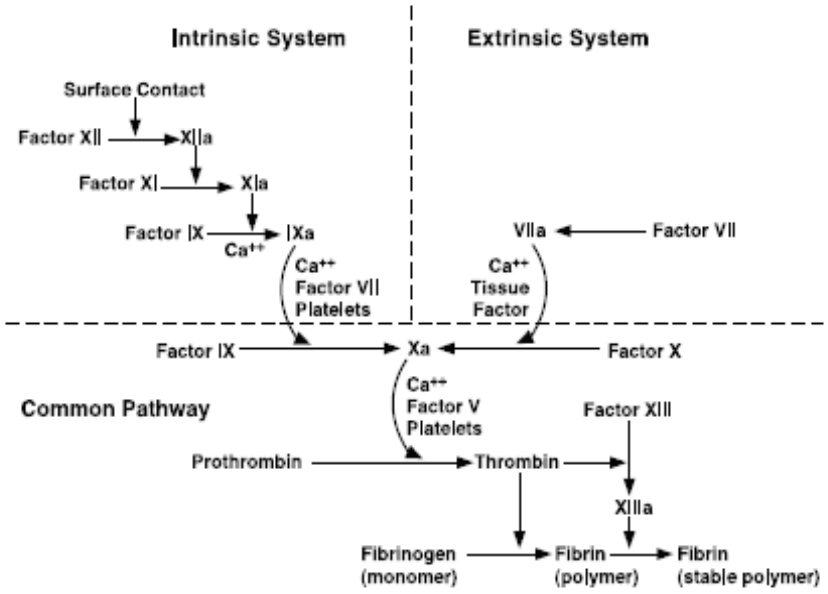

Figure 2-14 Blood coagulation. Clotting factors (proenzymes), identified by Roman numerals, interact in a sequential series of enzymatic activation reactions (coagulation cascade) leading to the amplified production of the enzyme thrombin, which in turn activates fibrinogen to form a fibrin polymer that stabilizes the clot or thrombus. [1]

2.7 Interaction of silk with blood plasma

The interaction between plasma protein and fibroin materials is a key point for the development of silk fibroin hemostatic wound dressings. At present, there is only limited published data on the adsorption of proteins to fibroin fibers [58]. Previously, Minoura et al. confirmed that the fibroin films support fibroblast adhesion [50], moreover, they have been modified to improve their physic-chemical properties and to make them inert towards cell adhesion [34, 85]. Recently, Santin et al. reported that the binding of fibrin(ogen) to fibroin

fibers and regenerated films [42, 51]. They established an in vitro method, in particular, the fibroin specimens were incubated in a solution of isolated fibrinogen containing thrombin and Factor XIII. As mentioned earlier, the thrombin activates the polymerization of the fibrinogen into the fibrin, while Factor XIII induces the crosslinking of fibrin fibrils to form clot [86]. The experiments were carried out in the presence and absence of calcium to investigate the role of calcium-dependent enzymes in the binding process. Judging from the SEM, the fibroin films did not show any visible fibrin polymerization, whereas the fibroin fibers were bound to the fibrin bundles through regularly spaced binding sites by a calcium-independent mechanism (Figure 2-15). Furthermore, they carried out surface modification of the silk fibers by treatment with formaldehyde [51]. Diluted solutions of formaldehyde were used with the goal of creating spacing arms covalently linked to the fibroin through the formation of Schiff's bases which would block the amino groups on the protein [87]. The formed imide groups would protrude towards the aqueous medium and be reduced to alcohols, thus conferring a more hydrophilic character to the fiber surface. Although no characterization was carried out to assess the surface modification produced by formaldehyde, this treatment dramatically inhibited fibrin(ogen) binding to the fibroin fibers; in a few non-representative areas only poorly bound polymerized clots to the fibroin fibers were observed. These results indicate that the presence of regularly spaced hydrophobic domains on the native structure of the silk fibroin is able to establish interactions with the polymerizing fibrinogen (Figure 2-16).

In the similar way, Motta et al. demonstrated that serum protein adsorption onto silk fabrics and films dramatically changes when the conformation of the silk fibroin is

rearranged by engineering procedures [52]. The serum proteins adsorption onto the native silk fibroin fibers and regenerated silk fibroin films showed different hydrophobic binding strength for the two materials, with the protein binding being greatest for the more hydrophobic fibroin fibers [52].

Since β-sheet structure is stabilized by hydrogen bonding, it was hypothesized that the fibers tend to expose non-polar amino acid side chains thus generating a relatively hydrophobic surface. As a result, native fibroin fibers seem to bind the serum proteins through strong hydrophobic interactions, most probably due to the orientation of fibroin hydroxyl groups towards the core of the protein to form the β-sheet hydrogen bonding. On the other hand, when the fibers were treated with chaotropic salt solutions (9.3M LiBr), the destabilizing ions disrupted the hydrogen bonding and induced the transition of the protein from an ordered crystalline structure (silk II) to a random coil conformation (silk I) [60]. The corresponding film cast by the solvent evaporation did not re-establish a significant number of β-sheets and the methanol treatment allowed only a partial formation of new β-sheets [8,14]. As a result of the protein denaturation, the regenerated fibroin films were more likely to expose a surface more hydrophilic to the external environment than the fibers, resulting in less binding with the protein.

These results support the concept that there would be specific fibrin(ogen) binding sites on fibroin fibers and hydrophobic β-sheet rich domains on the fiber surface could be able to interact with the polymerizing fibrinogen [51]. In conclusion, the β-sheet structure

seems to give fiber surface hydrophobicity that leads to stronger serum protein binding [51, 52].

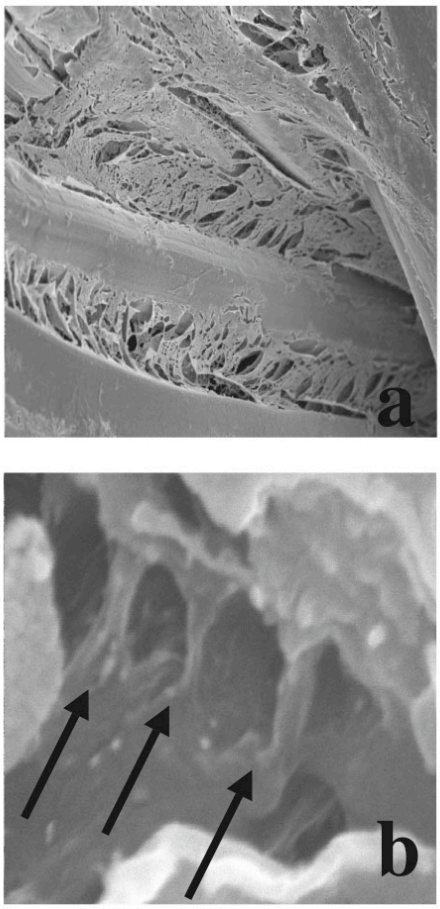

Figure 2-15 Cryo-SEM of the fiber/clot interface after incubation of fibroin fabric in polymerizing fibrin in presence of calcium. (a) laminar structures bridging fibers (x1500); (b) bundles contacting a fiber (x50000). Arrows indicate the morphology of the contact points. [51]

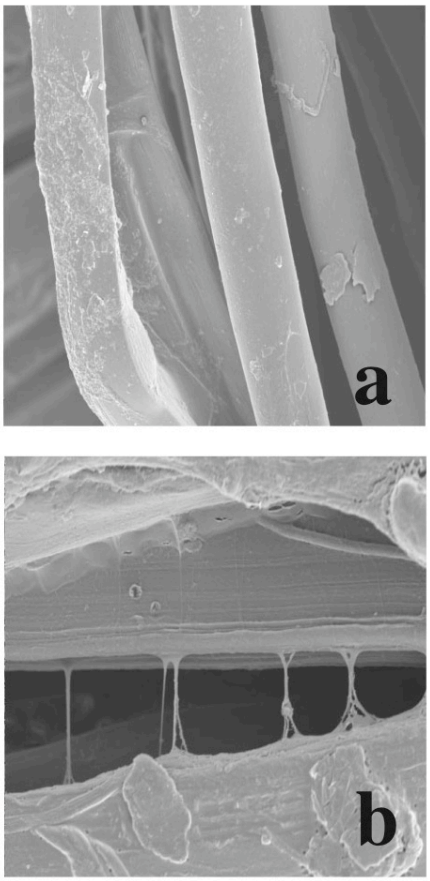

Figure 2-16 Cryo-SEM of formaldehyde-treated fibroin fibers after incubation in polymerizing fibrin in the presence of calcium, (a) unconditioned surfaces (x1500), (b) rare areas of interactions between the two polymers(x3000).[51]

2.8 Hemostasis evaluations

It is important to establish an easy method for the quantitative determination of the efficacy of local hemostatic dressings. Various methods have been proposed for the evaluation of hemostasis efficacy. The common parameters for *in vitro* examination of the blood clotting ability are hemoglobin concentration, platelet count, blood coagulation time (BCT), prothrombin time [88], activated partial thromboplastin time and plasma fibrinogen concentration are evaluated [89, 90]. Currently, prothrombin time (PT)[88], partial thromboplastin time (PTT), thrombin time (TT), activated partial thromboplastin time (APTT), clot retraction time (CRT), plasma recalcification time (PRT) [91], and whole blood clotting time (WBCT) [91-93] are commonly used to evaluate extrinsic coagulation systems. Similar coagulation tests, fibrin clot formation time, R_{APTT}, R_{TT}, R_{PT} values (ratio of APTT, TT or PT to those of the control assays) [94, 95], have been reported. Platelet aggregation (PA) is one of the key phenomena in blood coagulation. Tamada et al. reported a platelet rich plasma (PRP) method [96]. In this method, the number of platelets adhering to sample fabrics was calculated from the amount of lactate dehydrogenase (LDH) released from adhering platelet. Measurement of D-dimer concentration is also used to evaluate thrombosis. The D-dimer is a cross-linked fibrin degradation product and is used to identify excessive fibrinolysis in pathologic states. Furthermore, Prior et al. proposed a method wherein estimates of total bleeding derived from the weight gained by the preweighed gauze squares or cotton swabs was used to absorb uncoagulated blood from the surgical field of a rabbit kidney [97].

In addition, the erythrocyte sedimentation rate (ESR), also called a sedimentation rate, is the rate at which red blood cells precipitate in a period of an hour. It has been widely used for one of the diagnosis of various diseases [98]. In this method, anti-coagulated blood is placed in an upright tube, known as a Westergren tube (2.5 x 300 mm) and the rate at which the red blood cells fall is measured and recorded in mm/hour. The ESR is governed by the balance between pro-sedimentation factors, mainly fibrinogen, and those factors resisting sedimentation, namely the negative charge of the erythrocytes. When an inflammatory process is present, the high proportion of fibrinogen in the blood causes red blood cells to stick to each other. The red cells form stacks called rouleaux, which settle faster. Rouleaux formation can also occur in association with some lymphoproliferative disorders in which one or more immunoglobulins are secreted in high amounts. Rouleaux formation can, however, be a normal physiological finding in horses, cats and pigs [99, 100].

Test methods and results vary on collection of the blood specimen. None of these methods are, however, satisfactory for the quantitative determination of the efficacy of local hemostatic agents due to following reasons: they (1) do not simulate the actual situation where local hemostatic agents are clinically used or (2) do not present quantitative evaluations, or (3) necessitates complicated procedures [101].

3. PHYSICAL MODIFICATION OF SILK FIBERS

3.1 Introduction

The original silk fibroin has β-sheet crystalline structure with the crystallinity of 70%. The strong covalently bonded molecular chains are nearly fully extended and bonded with each other by hydrogen bonding between carbonyl oxygen and amide hydrogen, giving the β-sheet crystalline structure great strength. Moreover, the bonding between the β-sheets involves only weak van der Waals interactions between the side groups, resulting in the flexibility of the fiber. Due to these characteristic structural features, the original silk fibers have great mechanical properties.

When we consider their application for hemostatic wound dressing, the silk fibers should be modified to more desired form as dressing, such as more water absorbability, biodegradability, or strong interaction with blood plasma. For this objective, we assumed that the decrystalization of the β-sheet crystalline structure is required to improve/enhance water absorbability and biodegradability. This chapter discusses the decrystallization of the silk fibers. Some solvent systems were investigated their effect on the crystal structure of silk fibroin. Chemical and physical characterization were performed using Fourier transformed infrared spectroscopy (FTIR) and X-ray. The physical properties of the fibers were also analyzed by a tensile test and compared to the original or native silk fiber. The morphology of the fibers was examined by SEM.

3.2 Experimental

3.2.1 Materials

Grade 5A raw silk with an average denier of 20.86 produced in Brazil by the Fiaçào de Seda Bratac S.S. was used for this research. Raw silk was degummed prior to experiments by following a previously published method [105]. Sericin was removed with 0.25 % (w/v) sodium lauryl sulfate and 0.25% (w/v) sodium carbonate in boiling water, bath ratio of 1:100(w/v), for 1 hour. After the degumming, fibroin was washed in boiling water for 1 hour to remove remaining sericin and surfactants and then washed again with distilled water. The sericine fraction was calculated as 0.229.

All other chemicals for dissolving fibroin, such as calcium nitrate and methanol, were purchased from Fisher Scientific as reagent grades and used without further purification.

3.2.2 Preparation of solvent system

Calcium nitrate tetra-hydrate [$Ca(NO_3)_2\ 4H_2O$] was dissolved in methanol or ethanol at room temperature to prepare solutions with concentrations of 10% (w/w), 25% (w/w), 50% (w/w), 75% (w/w), and 90% (w/w). In the same manner, calcium chloride [$CaCl_2$] was dissolved in methanol or ethanol with concentration of 10 % (w/w), 25% (w/w), and 50% (w/w).

3.2.3 Decrystallization of silk fiber in the solvents

The degummed silk fibers (1 wt%) were immersed into the prepared solutions to decrystallize crystalline β-sheet conformation. Immersing time was varied from 5 min up to

300 min at room temperature and at 65℃ (above boiling point of methanol) in oil bath. After a certain time, the fibers were removed from the solutions and rinsed in deionized water then towel-dried. If there is no described condition, the fibers were treated at room temperature for 2 hours.

3.2.4 X-ray Diffraction (XRD)

The X-ray scans of degummed silk and treated silk fibers were obtained with a Seimens type F X-ray diffractometer. Ni-filtered Cu Kα radiation was used for the X-ray source with 35 kV voltage and 25 mA current. All scans were performed from 5 ° to 40 ° (2θ) at a speed of 1.0°/min.

3.2.5 Fourier Transform Infrared-Attenuated Total Reflectance (FTIR-ATR) spectroscopy

FTIR spectra of all samples were obtained using Nicolet 510P FT-IR Spectrometer with OMIIC software. Attenuated Total Reflectance (ATR) accessory was used for the spectra of the degummed silk fibers and treated fibers in solvents. All scans were performed with an average of 32 repeated scans from 4000 to 400 cm^{-1}.

3.2.6 Tensile tests

The fineness of the fibroin fiber samples was measured by a VIBROMAT®. The denier values of each sample were obtained as the average of 10 replicate measurements using a 50mg load cell. Tensile testing was conducted using a MTS Q-Test™ with 50g load

cell based on the obtained denier values. The separated single fiber was clamped at a gauge length of 1 inch (25.40 mm) and the tensile test was conducted at a rate of 15 mm/min. The data was converted to the corresponding tensile stress-strain curve. The values of energy, tensile stress, and tensile strain at break were measured, respectively. Tests were carried out under the condition of 20℃, 65% RH. At least five replicates were obtained for each sample. The values for peak load (gf) at break were converted into peak stress (MPa) using the following equation:

Peak Stress (MPa) =Force/Area (N/mm^2)

$$= \frac{load \times 0.009807(N)}{denier \Big/ 9000(m) \times density \times 10^6 (g/m^3)}$$

,where cross-section area of silk fiber $= \dfrac{denier(g/9000m)}{9000m \times density(g/cm^3)}$

$$= \frac{denier}{9000m \times density \times 10^6 (g/m^3)}$$

Thus,

$$\text{Peak Stress} = \frac{load \times 88.3(Nm) \times density(g/m^3) \times 10^6}{denier} (Nm^{-2})$$

$$= \frac{load \times 88.3 \times density}{denier} (MPa)$$

,where density of the silk fiber 1.353 g/cm^3 was used.

The values of peak elongation at break (mm) were converted into peak strain (%) using the following equation:

Strain (%) = Change in length (mm)/gauge length (mm) x100

Finally, the initial tensile modulus of each specimen was determined using following equation:

Initial modulus (GPa) = Stress (MPa)/ Strain

3.2.7 Moisture absorption test

The degummed silk fibers and treated fibers in $Ca(NO_3)_2$ $4H_2O$/MeOH solutions were dried in vacuum oven at 80℃ overnight and weighed. Then, they were place at 20℃, 65% RH and weighed again at predetermined time interval. Moisture regain was calculated for each sample.

3.2.8 Scanning Electron Microscopy (SEM)

Various silk fibers were examined by the FEI scanning electron microscope (SEM). The samples were sputter-coated with gold by plasma in order to minimize electron charging on the surface and to obtain fine images. Their surface morphology was examined.

3.3 Results and Discussion

3.3.1 Characterization of silk fibers treated in $Ca(NO_3)_2$ $4H_2O$/ MeOH

The degummed silk obtained after removing the outer sericin has been reported to consist of silk II structure, which contains β-sheet crystal [103]. For reference, the signature

FTIR spectrum of original silk fibroin that possesses the β-sheet conformation (silk II) exhibits the following peaks [32, 70]: amide I (1625 cm^{-1}), which is related to the stretching of C=O groups in silk fibroin back bone, amide II (1520 cm^{-1}), which is representative of the N-H deformation in silk fibroin amide groups, and amide III (1265 cm^{-1}), which arising from the vibration involving O-C-O and N-H. The amide I peak shifts from 1625 cm^{-1} to 1655 cm^{-1}, and the amide II peak shifts from 1520 cm^{-1} to 1545 cm^{-1}, corresponding with transition of the silk from β-sheet crystalline conformation (silk II) to random coil conformation (silk I). The amide III peak is characteristic for only silk II conformation.

To investigate the effect of prepared solvent systems on β-sheet crystalline structure of silk fibroin, FTIR spectra of treated silk fibers in the $Ca(NO_3)_2$ $4H_2O$/MeOH solutions for 2 hours at room temperature were obtained and compared with those of the non-treated degummed silk fibers. Figure 3-1 shows FTIR spectra of the degummed silk fibers and treated silk fibers in the solutions, varying the concentration from 10% (w/w) to 90% (w/w). The FTIR spectrum of the degummed silk fibers confirmed the presence of β-sheet conformation at each amide peak. Treated silk fibers in different concentration of the solutions showed almost the same profiles as that of the degummed silk in the spectra, exhibiting the absorption bands assigned to β-sheet crystalline structure at around 1655 cm^{-1} (amide I), 1545 cm^{-1} (amide II), and 1265 cm^{-1} (amide III), respectively. We could not confirm any shifts of the amide I peak and the amide II peak close to the characteristic values of random conformation (silk I), even though there were some differences in the absorbance between each fibers. This indicates that the β-sheet crystalline structure of the silk fibers

was somewhat decrystallized after the treatment in the $Ca(NO_3)_2$ $4H_2O$/MeOH solutions, however the obtained FTIR data were not sufficient to quantify the decrystallization.

Since the decrystallization by the $Ca(NO_3)_2$ $4H_2O$/MeOH solutions was less effective than we expected under the condition of room temperature, then the fiber solutions were incubated in oil bath at 65℃ for 2 hours, which above the boiling point of methanol. As shown in Figure 3-2, obtained FTIR spectra of silk fibers treated at 65℃ were different from those of treated silk fibers at room temperature. Significant shift of peak at 1520 cm^{-1} (amide II) was observed at each concentration of $Ca(NO_3)_2$ $4H_2O$/MeOH solution. Above 50% (w/w), the treated silk fibers clearly started to dissolve and showed different appearance. Moreover, silk fibers treated in 75% (w/w) and 90% (w/w) solutions dissolved perfectly.

Figure 3-3 shows the change in absorbance at 1630 cm^{-1} (amide I) in the FTIR spectra of the fibers treated in $Ca(NO_3)_2$ $4H_2O$/MeOH for 2 hours at room temperature and 65℃. At both temperatures, crystallinity of fibers treated in 10% (w/w) and 25% (w/w) solutions gradually increased and then started to decrease in 50%(w/w) solution. However, the absorbance started to increase again when the silk fibers were treated in 75% (w/w) and 90% (w/w) solutions. The fibers treated in 50% (w/w) solution at 65℃ exhibited lowest crystallinity, suggesting that the largest decrystallization of β-sheet conformation under this condition. On the other hand, the solutions with other concentrations might help methanol-induced formation of β-sheet crystalline formation, at least they do not work for decrystallization of the silk fibers effectively. This plot also showed that environment temperature enhanced the effect of the solvent system. At high temperature, silk fibroin

chains can rotate and give more free space so that the solvent might easily diffuse and induce the conformational change of silk fibroin molecules. Thus, combination of high concentration of solution and high temperature causes more effective and rapid decrystallization. The notable thing is that the crystallinity of fibers treated in 75% (w/w) and 90% (w/w) at room temperature started to increase again. This is an unexpected result for us and we could not sufficiently explain this behavior based on only FTIR.

As mentioned earlier, methanol has been reported to induce crystallization of silk fibroin [32, 68, 70]. Gil et al. [106, 107] revealed that in methanol-induced silk fibroin crystallization, most of the β-sheet conformation occurs during the first 5 minutes of exposure to MeOH/water (75/25 w/w) at 20℃ [32]. Based on this previously reported result, FTIR spectra were obtained to investigate the effect of treatment time period in 75% (w/w) $Ca(NO_3)_2$ $4H_2O$/MeOH solution at room temperature. Treatment time period varied from 5 min to 300 min. Figure 3-4 indicates that there were no difference in spectra between the fibers treated for 5 min and the fibers treated for 300 min. These show that these time periods (max. 300 min) are not enough for fibers to cause significant difference in their structure in the 75% (w/w) solution.

The X-ray diffraction curves of the degummed silk and the treated silk fibers in $Ca(NO_3)_2$ $4H_2O$/MeOH solutions for 2 hours at room temperature are shown in Figure 3-5. According to previous study [105], a major peak at $2\theta = 21^\circ$ and two minor peaks at $2\theta = 9^\circ$ and 24° are assigned as characteristic peaks of the β-sheet crystalline structure. Although the treated silk fibers still showed the peaks of the β-sheet crystal structure similar to that of the

degummed silk, the size and perfection of the β-sheet crystal structure as well as the degree of crystallinity were lower compared with the degummed one. The peak intensity values at 2 θ =21° of the samples were used to indicate changes in the crystallinity of them. As shown in Figure 3-5**,** crystallinity tended to increase for the silk fibers treated in 10% (w/w) and 25% (w/w) solutions, compared with that of the degummed silk. Then, the crystallinity started to decrease and showed lowest value for the fibers treated in 50% (w/w) solution, suggesting that decrystallization of silk started at this concentration. However, when the concentration of the solution was increased to 75% (w/w) and 90% (w/w), the crystallinity tended to increase again. The appearance of these fibers seemed to become less flexible and more delicate than the untreated degummed silk.

Next, crystallinity of the silk fibers treated in the same solutions for 2 hours at 65℃ were measured by X-ray diffraction (Figure 3-6). The peak intensity at 2 θ =21° increased with the treatment in 10% (w/w) and 25% (w/w) solutions, then started to dramatically decrease when the fibers were treated in 50% (w/w) solution. The silk fibers were partially dissolved in 50% (w/w) solution and perfectly dissolved above the concentration of 50% (w/w). These results were totally consistent with the results of FTIR and clearly showed that higher temperature helps the solvent decrystallize the silk fibers. We consider that the solvent molecules diffused easily into the amorphous region (free volume) of the silk fibroin fiber and disrupted its crystalline structure by forming new hydrogen bonds with the fibroin molecules.

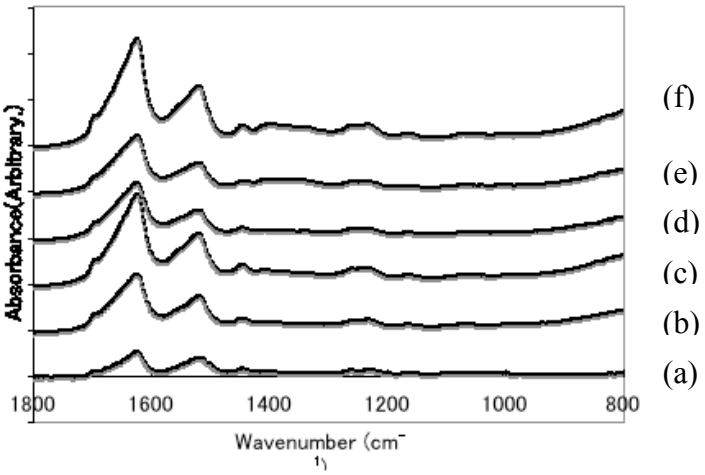

Figure 3-1 FTIR-ATR spectra of treated silk fibers in $Ca(NO_3)_2$ $4H_2O$/MeOH for 2 h at room temperature; (a) degummed silk, treated in (b) 10%(w/w), (c) 25% (w/w), (d) 50%(w/w), (e) 75%(w/w), (f) 90% (w/w).

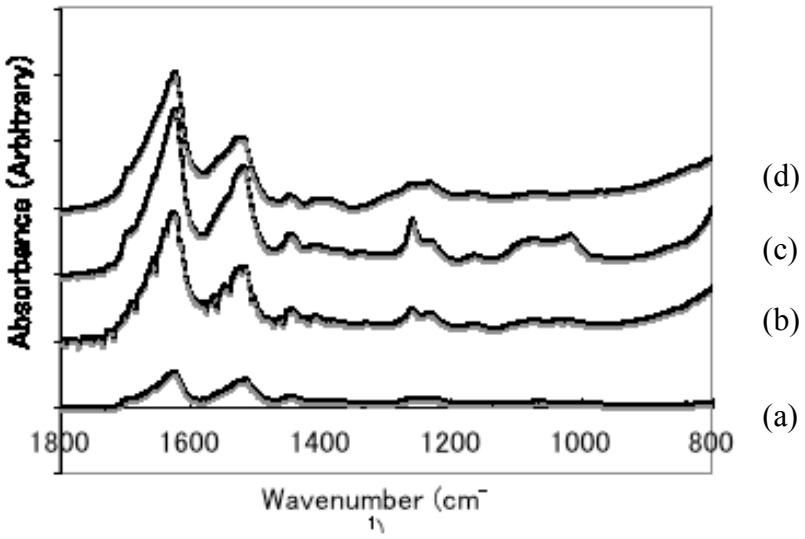

Figure 3-2 FTIR-ATR spectra of treated silk fibers in $Ca(NO_3)_2$ $4H_2O$/MeOH for 2 h at 65℃; (a) degummed silk, treated in (b) 10% (w/w), (c) 25% (w/w), (d) 50% (w/w).

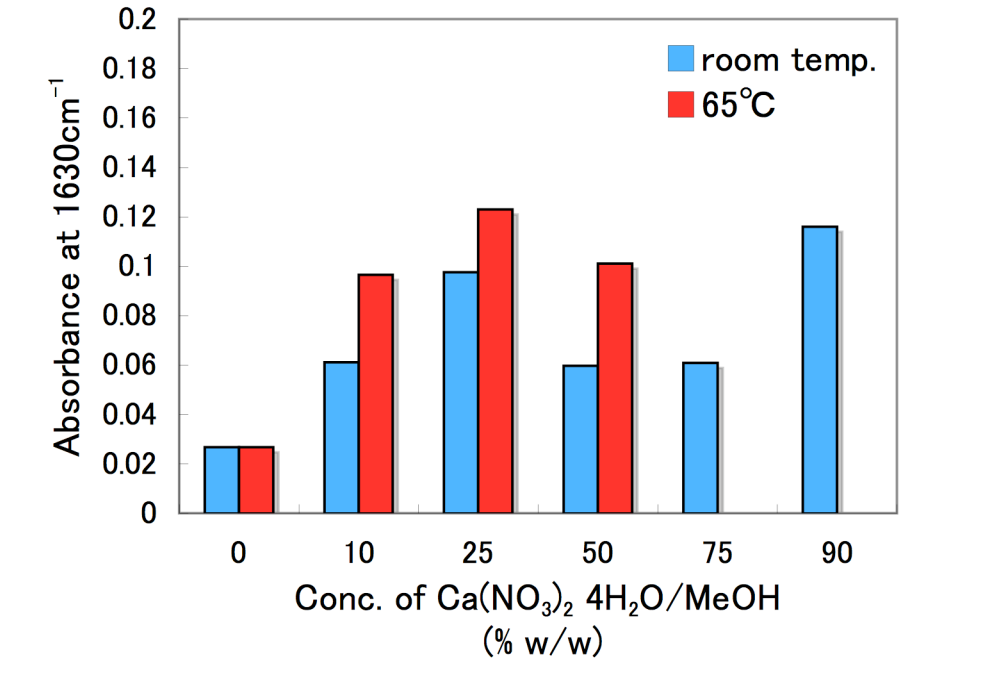

Figure 3-3 The absorbance at 1630 cm^{-1} of treated silk fibers in Ca(NO$_3$)$_2$ 4H$_2$O/MeOH for 2 h at room temperature and at 65℃.

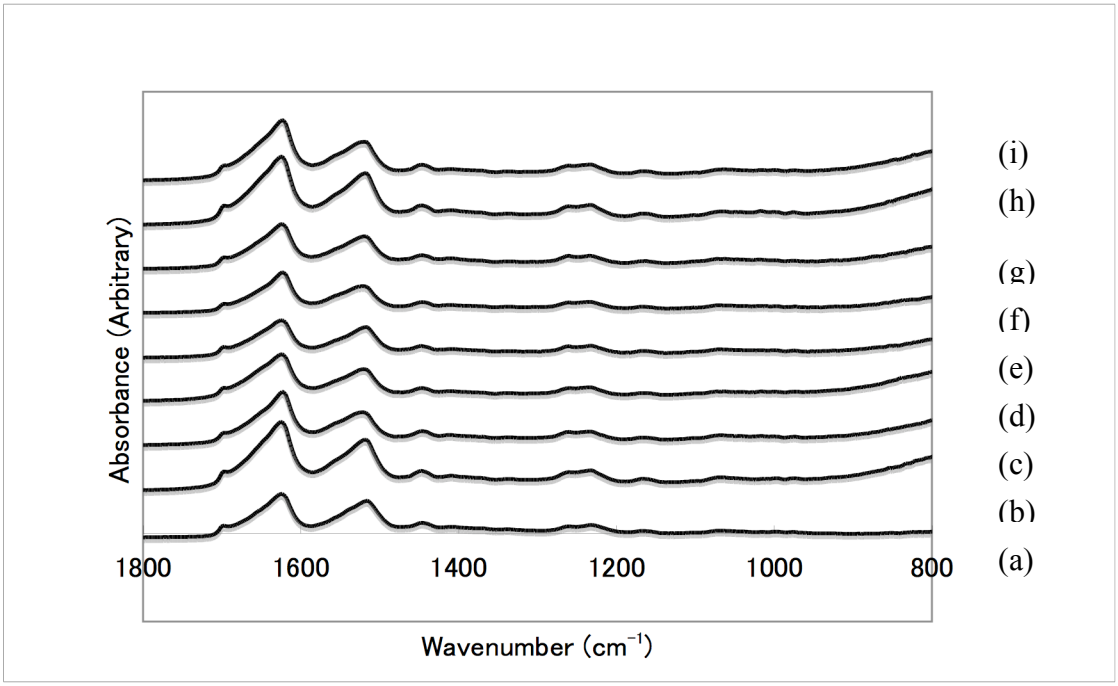

Figure 3-4 FTIR-ATR spectra of treated silk fibers with different treatment time in 75% (w/w) $Ca(NO_3)_2$ $4H_2O$/MeOH; (a) degummed silk (b) 5 min, (c) 15 min, (d) 30 min, (e) 60 min, (f) 90 min, (g) 120 min, (h) 150 min, (i) 300 min.

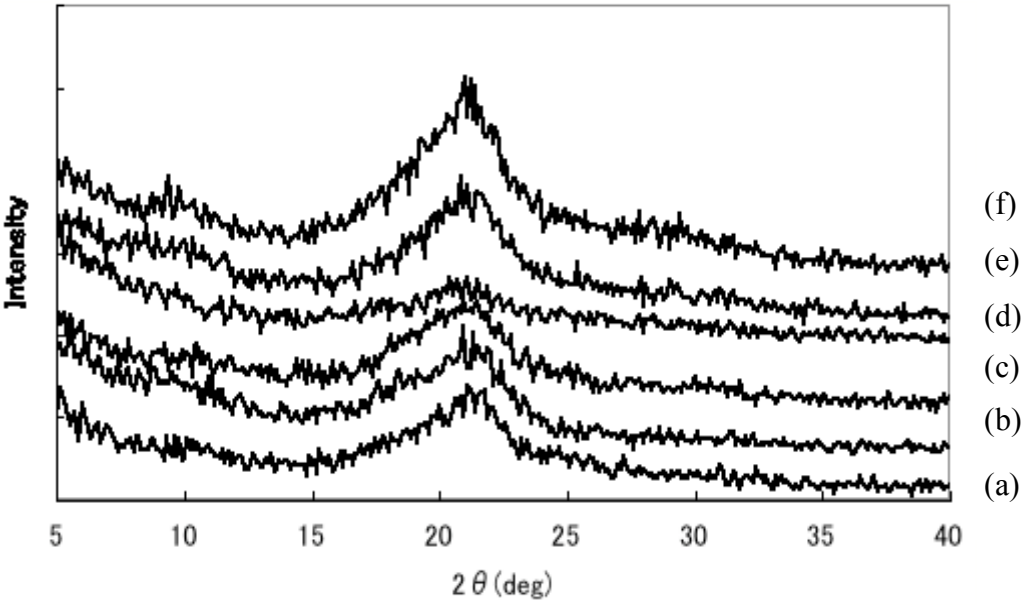

Figure 3-5 X-ray Diffraction (XRD) curve of treated silk fibers in $Ca(NO_3)_2$ $4H_2O$/MeOH for 2 h at room temperature; (a) degummed silk, (b) 10% (w/w), (c) 25% (w/w), (d) 50% (w/w), (e) 75% (w/w), (f) 90% (w/w).

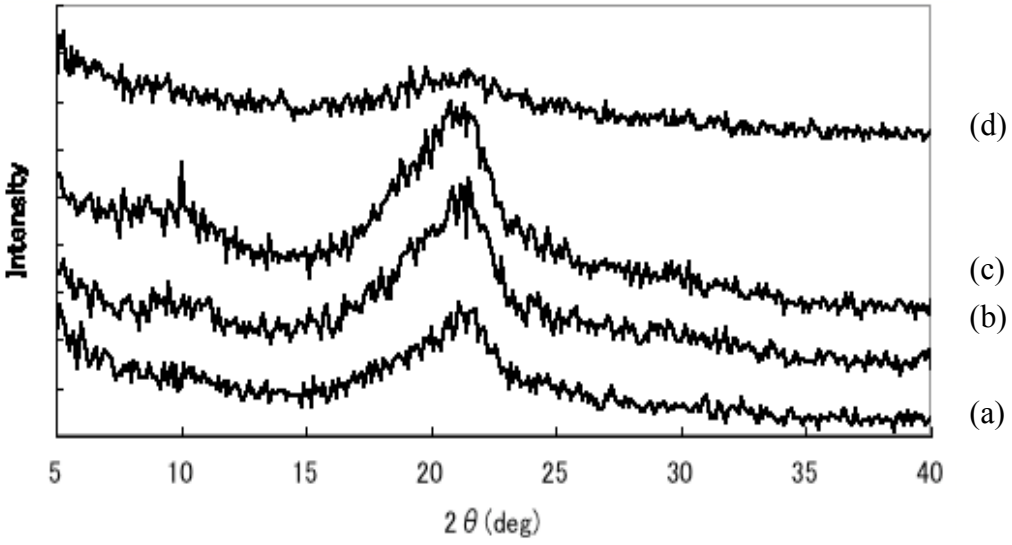

Figure 3-6 X-ray Diffraction (XRD) curve of treated silk fibers in $Ca(NO_3)_2$ $4H_2O$/MeOH for 2 h at 65℃; (a) degummed silk, (b) 10% (w/w), (c) 25% (w/w), (d) 50% (w/w).

3.3.2 Characterization of silk fibers treated in $Ca(NO_3)_2$ $4H_2O$/ EtOH

Solutions of $Ca(NO_3)_2$ $4H_2O$/EtOH, varying in concentration from 10% (w/w) to 90% (w/w), were also used in the same manner to investigate the difference between methanol and ethanol in the calcium nitrate system. As shown in Figure 3-7, FTIR spectra of treated silk fibers in $Ca(NO_3)_2$ $4H_2O$/EtOH solutions for 2 hours at room temperature exhibited few shifts of the amide I peak and the amide II peak. In addition, the crystallinity of the treated silk fibers was also measured by X-ray diffraction (Figure 3-8). The peak intensity at $2\theta = 21^\circ$ tended to increase with the increase in the concentration up to 75% (w/w), then gradually started to decrease for the fibers in 90% (w/w) solution. The results of FTIR and X-ray demonstrated that $Ca(NO_3)_2$ $4H_2O$/EtOH is less effective than $Ca(NO_3)_2$ $4H_2O$/MeOH. Ha et al. [27] reported the complex model consists of $Ca(NO_3)_2$ $4H_2O$/MeOH and silk fibroin, and there might be specific compatibility between these two materials, even though detail mechanism has not been clear. None of the ethanolic solutions dissolved the native silk fibers.

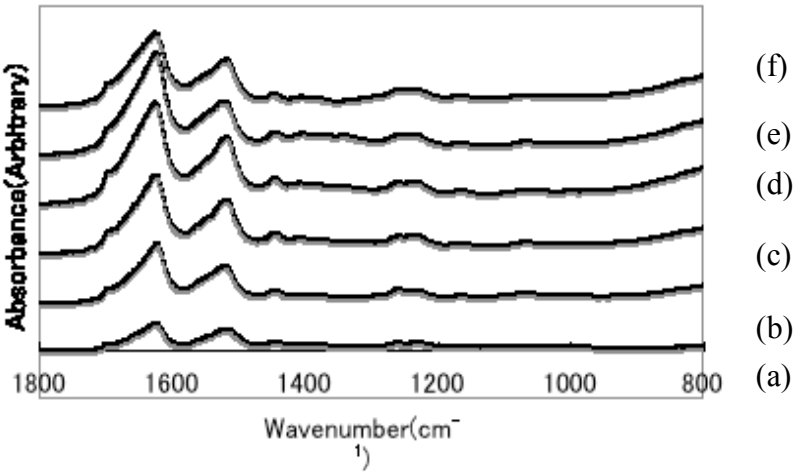

Figure 3-7 FTIR-ATR spectra of treated silk fibers in $Ca(NO_3)_2$ $4H_2O$/EtOH for 2 h at room temperature; (a) degummed silk, (b) 10% (w/w), (c) 25% (w/w), (d) 50% (w/w), (e) 75% (w/w), (f) 90% (w/w).

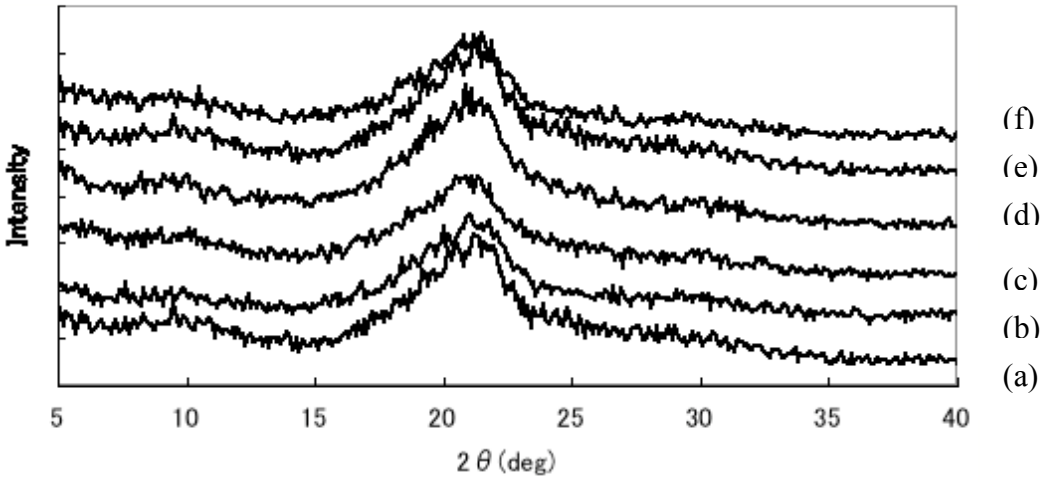

Figure 3-8 X-ray Diffraction (XRD) curve of treated silk fibers in $Ca(NO_3)_2$ $4H_2O$/EtOH for 2 h at room temperature; (a) degummed silk, (b) 10% (w/w), (c) 25% (w/w), (d) 50% (w/w), (e) 75% (w/w), (f) 90% (w/w).

3.3.3 Comparison $Ca(NO_3)_2$ $4H_2O$/MeOH and $Ca(NO_3)_2$ $4H_2O$/EtOH

Comparing the FTIR spectra, the silk fibers exhibited different conformation change in methanol system and ethanol system. In both systems, crystallinity showed a minimum value at 50% (w/w) solution. However, the crystallinity of the fibers in $Ca(NO_3)_2$ $4H_2O$/MeOH increased gradually with the increase in concentration of the solution up to 75% (w/w), on the other hand, the fibers in $Ca(NO_3)_2$ $4H_2O$/EtOH started to decrease in 90% (w/w) solution. The comparison of peak absorbance values at 1630 cm^{-1} between these two solvent systems gives the information about how they affect the crystalline structure of silk fibroin. The results show that $Ca(NO_3)_2$ $4H_2O$/MeOH solution is more effective than ethanol system to decrystallize silk fibroin in our research (Figure 3-9).

From the full width at half maximum intensity of the peak (FWHM) in the X-ray diffraction, the crystallite size *d* can be estimated using the Scherrer equation:

$$d = 0.9\,\lambda / (B \cos\theta)$$

where λ is the wavelength of radiation, B is the peak full width at half maximum (FWHM), and θ is the scattering angle. Table 3-1 (a), (b) shows the results of this analysis. These values give us an average crystal size, however they say nothing about the crystal size distribution or spatial arrangement, both of which affect fiber properties. As shown in Table 3-1, calculated average crystal size in fibers treated in 50% (w/w) $Ca(NO_3)_2$ $4H_2O$/MeOH solution was much smaller than that in untreated degummed silk fibers or other fibers treated in different concentration of solutions or the different solvent. This result also supports that treatment in 50% (w/w) $Ca(NO_3)_2$ $4H_2O$/MeOH solution causes the decrystallization of silk fibroin most effectively.

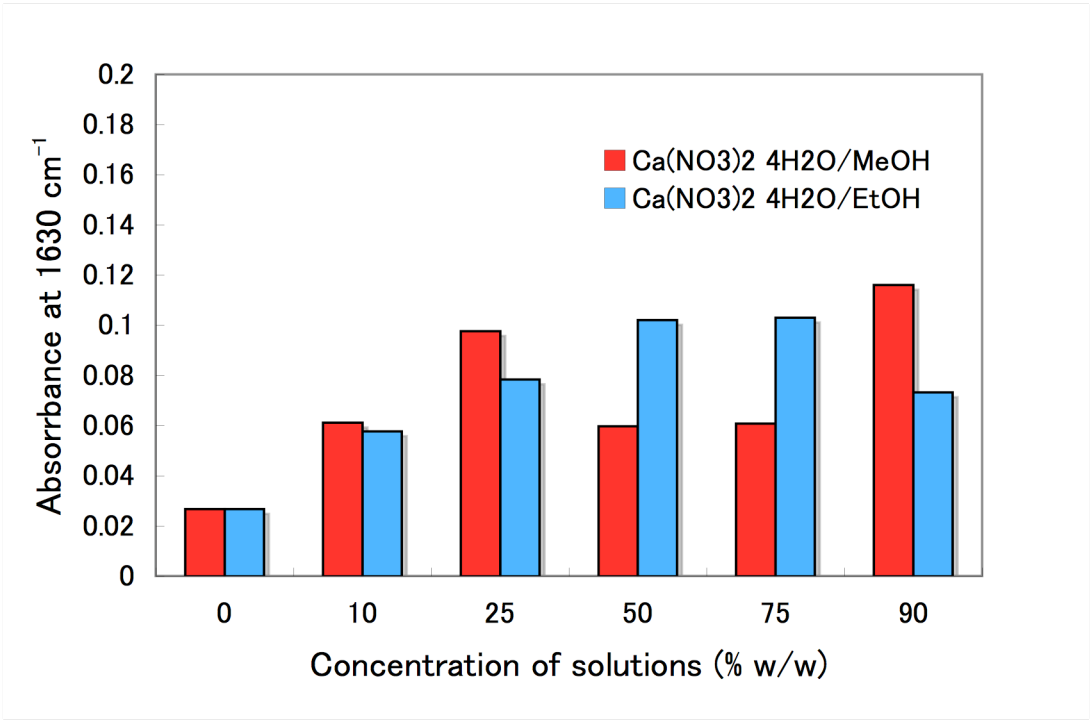

Figure 3-9 The absorbance at 1630 cm^{-1} of treated silk fibers in $Ca(NO_3)_2$ $4H_2O$/MeOH and $Ca(NO_3)_2$ $4H_2O$/EtOH for 2 h at room temperature.

Table 3-1 (a) Crystal size determined by the Scherrer equation* of the degummed silk fibers.

	2 θ at peak (deg)	FMWH (deg)	Crystal size (nm)
Degummed silk	21.23	5.85	1.37

Table 3-1 (b) Crystal size determined by the Scherrer equation* of the treated silk fibers in $Ca(NO_3)_2$ $4H_2O$ systems.

Treatment Condition	**$Ca(NO_3)_2$ $4H_2O$/MeOH**			**$Ca(NO_3)_2$ $4H_2O$/EtOH**		
	2 θ at peak (deg)	FMWH (deg)	Crystal size (nm)	2 θ at peak (deg)	FMWH (deg)	Crystal size (nm)
10% (w/w) at R.T.	21.00	4.85	1.65	20.95	5.93	1.35
25% (w/w) at R.T.	20.38	5.85	1.37	20.93	5.68	1.41
50% (w/w) at R.T.	20.77	8.46	0.95	20.74	5.34	1.50
75% (w/w) at R.T.	20.78	4.77	1.68	20.93	5.76	1.39
90% (w/w) at R.T.	21.23	4.97	1.61	21.18	5.51	1.45
10% (w/w) at 65℃	21.69	4.91	1.63	-	-	-
25% (w/w) at 65℃	20.77	5.69	1.41	-	-	-
50% (w/w) at 65℃	20.77	10.92	0.73	-	-	-

* wavelength of radiation: λ =0.1542 nm

3.3.4 Characterization of silk fiber treated in $CaCl_2$/MeOH

As another solution system, the decrystallization of the degummed silk fibers in calcium chloride / methanol solutions ($CaCl_2$/MeOH) was tested and compared with the fibers treated in calcium nitrate systems. Figure 3-10 shows the FTIR spectra of the degummed silk fiber and fibers treated in $CaCl_2$/MeOH for 2 hours at room temperature, varying concentration of solutions from 10% (w/w) to 50% (w/w). Since $CaCl_2$ was almost saturated in 50% (w/w) solution, solutions of concentration above 50% (w/w) could not be obtained. As shown in the spectra, there were few differences between the treated fibers in different concentrations. Neither amide I peak or the amide II peak shifted to left, suggesting the very few transition from β -sheet conformation to random coil conformation.

As well as the $Ca(NO_3)_2$ $4H_2O$ systems, the silk fibers were also treated at 65℃. As shown in Figure 3-11, the fibers treated in 50% (w/w) solution at 65℃ exhibited lowest absorbance in its spectra, indicating that fibers were decrystallized under this condition. In fact, the fibers treated in 50% (w/w) were significantly partially dissolved. As a result, the absorbance at 1630 cm^{-1} was lower than that of the degummed silk fibers (Figure 3-12). However, we could not find out any appearance differences of the fibers treated between in $Ca(NO_3)_2$ $4H_2O$/MeOH solutions and in $CaCl_2$/MeOH solutions from the FTIR data.

The crystallinity of the silk fibers treated in $CaCl_2$/MeOH solutions were also tested using X-ray diffraction analysis. The X-ray diffraction curve of the degummed silk and treated silk are shown in Figure 3-13. There were not any significant differences observed between the silk fibers treated in 10% (w/w), 25% (w/w), and 50% (w/w) solutions at room

temperature, exhibiting almost the same peak intensity at 2 θ =21° . When the fibers were treated in the same solutions at 65℃, on the other hand, the peak intensity exhibited lower values at every concentration (Figure 3-14). Especially, the fibers treated in 50% (w/w) solution showed the lowest intensity. The treated fibers under this condition were almost dissolved and the collected fibers were fragile compared to the untreated fibers. Average crystal sizes were estimated using the Scherer equation and results are shown in Table 3-1 (c). Compared with the average crystal sizes of the silk fibers treated in $Ca(NO_3)_2$ $4H_2O$/MeOH as summarized in Table 3-1 (b), the average crystal sizes of fibers treated in $CaCl_2$/MeOH at room temperature and at 65℃!were more or less larger except the treatment in 10%(w/w) solution. For example, the average crystal sizes of silk fibers treated at room temperature were larger by 27% and by 70%, respectively, in 25%(w/w) and in 50% (w/w) $CaCl_2$/MeOH solutions than those of fibers treated $Ca(NO_3)_2$ $4H_2O$/MeOH with same concentrations, suggesting lower decrystallization ability of $CaCl_2$/MeOH than $Ca(NO_3)_2$ $4H_2O$/MeOH. At both temperatures, however, the average crystal size of fibers treated in 10% (w/w) $CaCl_2$/MeOH was slightly smaller than that of fibers treated in 10% (w/w) $Ca(NO_3)_2$ $4H_2O$/MeOH.

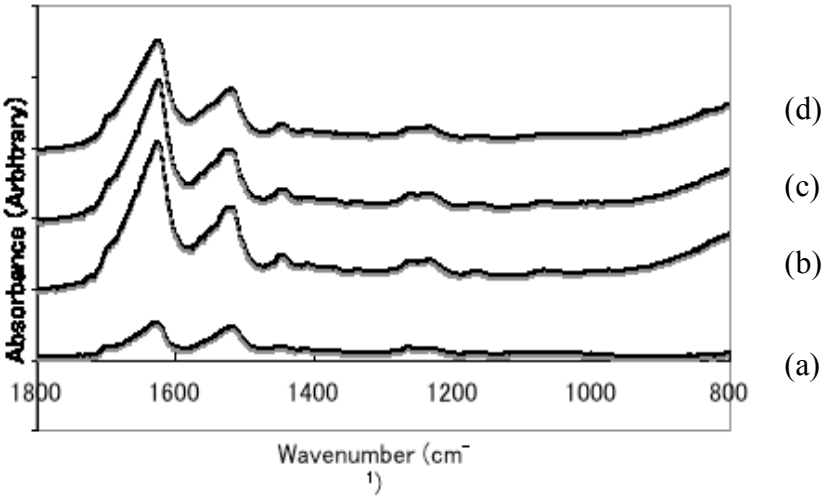

Figure 3-10 FTIR-ATR spectra of treated silk fibers in $CaCl_2$/MeOH for 2 h at room temperature; (a) degummed silk, (b) 10% (w/w), (c) 25% (w/w), (d) 50% (w/w).

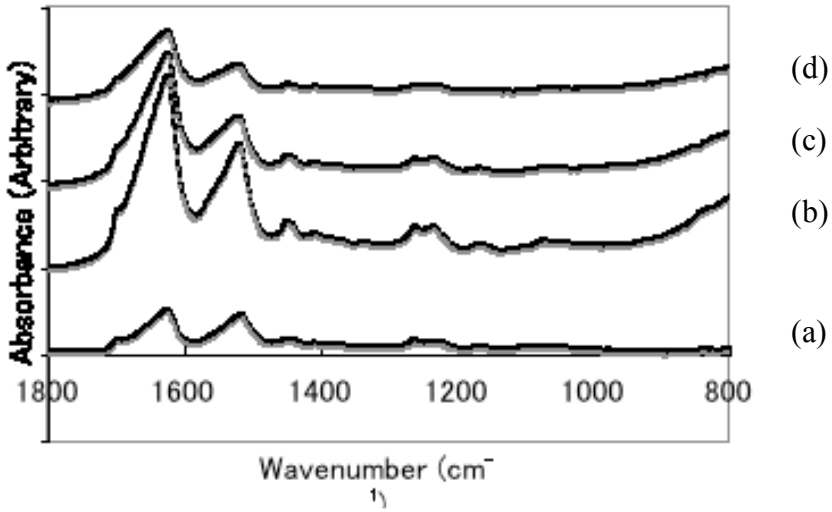

Figure 3-11 FTIR-ATR spectra of treated silk fibers in $CaCl_2$/MeOH for 2 h at 65℃; (a) degummed silk, (b) 10% (w/w), (c) 25% (w/w), (d) 50% (w/w).

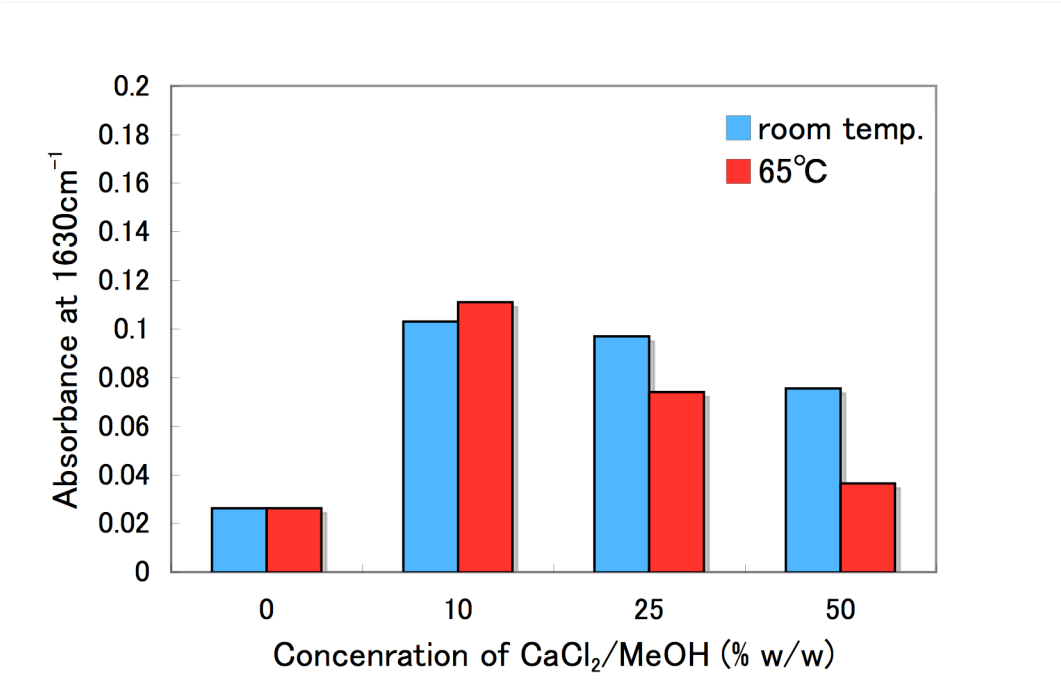

Figure 3-12 The absorbance at 1630 cm^{-1} of treated silk fibers in $CaCl_2$/MeOH for 2 h at room temperature and at 65℃.

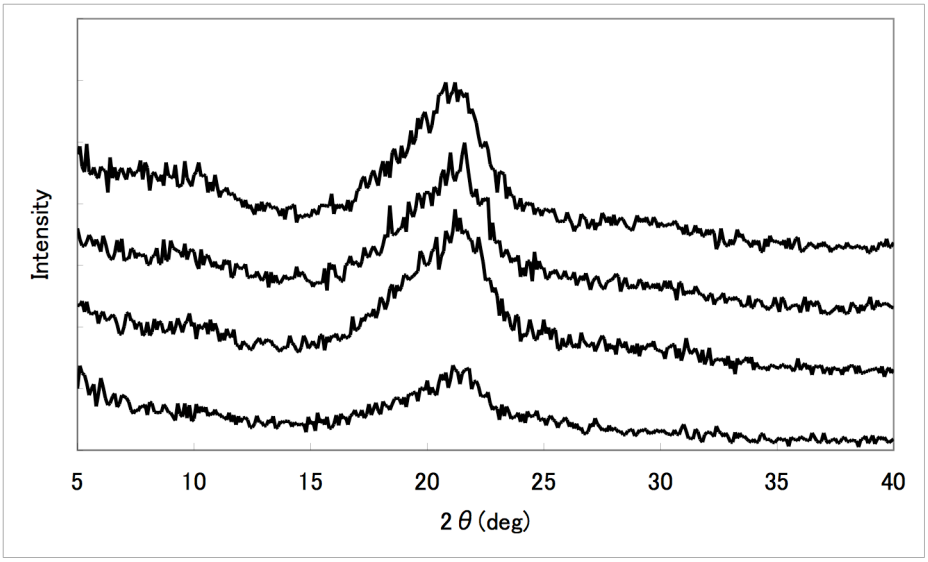

Figure 3-13 X-ray Diffraction (XRD) curve of treated silk fibers in $CaCl_2$/MeOH for 2 h at room temperature; (a) degummed silk, (b) 10% (w/w), (c) 25% (w/w), (d) 50% (w/w).

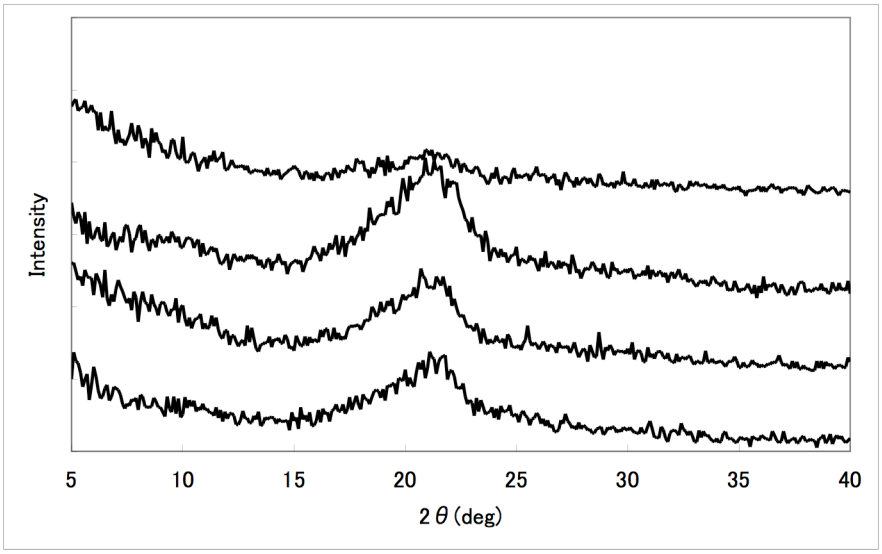

Figure 3-14 X-ray Diffraction (XRD) curve of treated silk fibers in $CaCl_2$/MeOH for 2 h at 65℃; (a) degummed silk, (b) 10% (w/w), (c) 25% (w/w), (d) 50% (w/w).

Table 3-1 (c) Crystal size determined by the Scherrer equation* of treated silk fibers in $CaCl_2$ systems.

Treatment Condition	**$CaCl_2$/MeOH**		
	2 θ at peak (deg)	FWHM (deg)	Crystal size (nm)
10% (w/w) at R.T.	21.23	4.91	1.63
25% (w/w) at R.T.	21.51	4.62	1.74
50% (w/w) at R.T.	21.00	4.94	1.62
10% (w/w) at 65℃	21.23	5.06	1.58
25% (w/w) at 65℃	21.08	5.000	1.60
50% (w/w) at 65℃	21.05	8.00	1.00

* wavelength of radiation: λ =0.1542 nm

3.3.5 Characterization of silk fiber treated in $CaCl_2$/EtOH

In the same manner, the effect of $CaCl_2$/EtOH on decrystallization of silk fibers were tested by FTIR as shown in Figure 3-15. The slight shifts of the amide II peak suggest the decrystallization of the treated silk fibers. From the peak absorbance at 1630 cm^{-1} (Figure 3-16), there were not any specific differences observed between the effect of $CaCl_2$ /MeOH and the effect of $CaCl_2$/ EtOH.

As mentioned in chapter 2, Ajisawa et al. [77] investigated that dissolution of silk fibroin was greatly improved in $CaCl_2/H_2O$/EtOH (molar ratio= 1:8:2) solution. They reported that the silk fibroin was insoluble in a solution of $CaCl_2/H_2O$ (molar ratio=1:8) at 20℃to 30℃(approx. room temp) for 240 to 720 hours, then solubility of silk fibroin in the aqueous solution increased to 0.7% to 3.3%, respectively, at 40℃ to 60℃ for 1hour.

However, when ethanol was added to the solution (molar ratio= 1:8:2), fibroin dissolved completely at 55℃ for 1 hour, which was approximately 35 times more likely than with the calcium aqueous solution [68, 77-80]. Their study supports our results that the treatment in $CaCl_2$/EtOH solution of 10% (w/w) (molar ratio =1:22) and 25% (w/w) (molar ratio= 1:7) at room temperature were not effective to decrystallize silk fibroin, on the other hand, the treatment in 50% (w/w) solution (molar ratio =1:2) at 65℃ for 2 hours caused best decrystallization behavior at this point. The molar ratio of calcium and ethanol is a key factor in the decrystallization of silk fibroin as well as the environment temperature. In our research, water was not added into $CaCl_2$/EtOH solution and the role in water has not been revealed. According to previous study [84], it has been reported that calcium/H_2O/methanol could make a complex with amide bond in Nylon 6. Therefore, water would somewhat contribute to the dissolution of silk. Further experiments with calcium/water/ethanol are needed for future work.

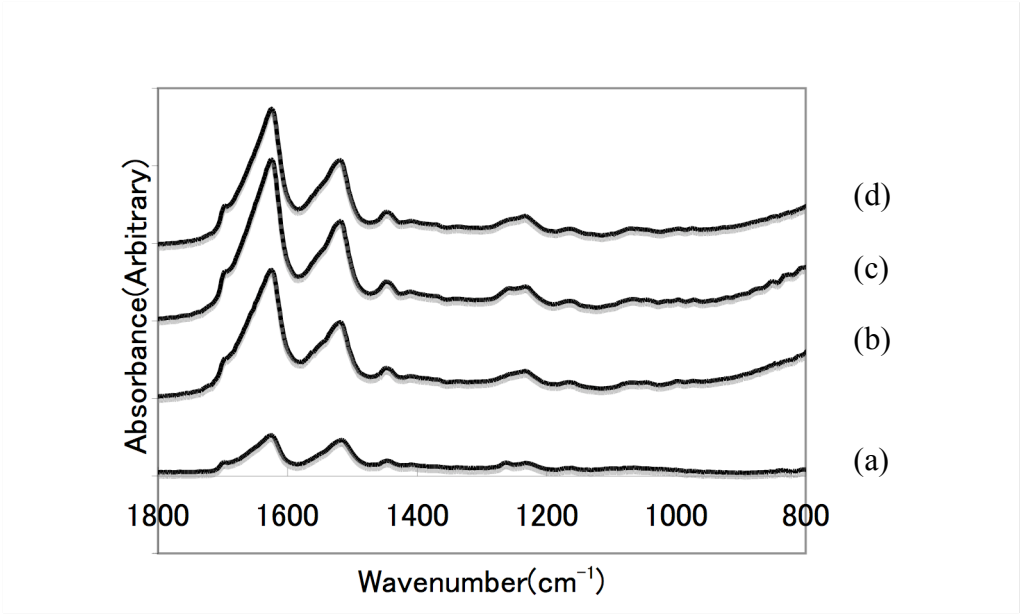

Figure 3-15 FTIR-ATR spectra of treated silk fibers in $CaCl_2$/EtOH for 2 h at room temperature; (a) degummed silk, (b) 10% (w/w), (c) 25% (w/w), (d) 50% (w/w).

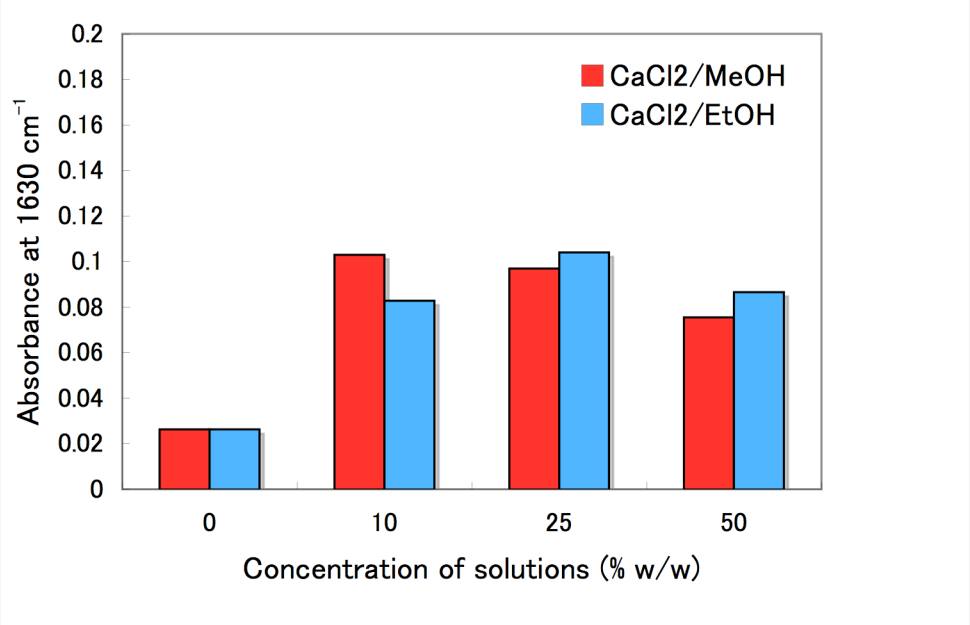

Figure 3-16 The absorbance at 1630 cm^{-1} of treated silk fibers in $CaCl_2$/MeOH and $CaCl_2$/EtOH for 2 h at room temperature.

3.3.6 Mechanical property of the treated silk fibers

Average deniers of the degummed silk fiber and treated silk fibers in $Ca(NO_3)_2$ $4H_2O$/MeOH solutions and their mechanical properties were measured. Previously Ha et al. [27] measured fineness of original silk fiber and regenerated silk fibers from various solvents as shown in Table 2-4 (a-c). The obtained deniers in this research were relatively consistent with the denier of original silk in Table 2-4(a). With the increase in concentration of $Ca(NO_3)_2$ $4H_2O$/MeOH solutions, the denier values of treated fibers slightly decreased, suggesting the partially dissolution of the fibers.

The variance of tenacity, peak stress, strain at break, and initial modulus of the degummed silk fibers and the treated silk fibers are listed in Table 3-2. The degummed silk fiber exhibited 3.83 gf/den tenacity, 23.04 % strain at break, and 2.04 GPa initial modulus, respectively. These values also relatively correspond with the reported tensile properties of the original silk fibers as shown in Table 2-2 and Table 2-4 (b). Compared with the data of the original silk fiber reported by Ha et al. (Table 2.4 (c)), it is seen that the fineness and mechanical properties were changed after the treatment in $Ca(NO_3)_2$ $4H_2O$/MeOH solutions, depending on the solvent concentration. As the concentration of $Ca(NO_3)_2$ $4H_2O$/MeOH solution increases, the tenacity and the initial modulus gradually increases and reached highest values at the fibers treated in 50% (w/w) solution, 4.13gf/den and 3.77 GPa, respectively, then started to decrease for the fibers treated in 75% (w/w) and 90% (w/w) solutions. On the other hand, the strain at break and toughness gradually decreased with the increase in the solution concentration. For the fiber treated in highest concentration solution of 90% (w/w) showed smallest strain at break of 16.26 % and toughness of 0.41 gf/den,

respectively. These results indicate that fibers treated in 50% (w/w) solution became more stiff and less flexible after they were immersed into the solvent. Moreover, the treated silk fibers in $Ca(NO_3)_2$ $4H_2O$/MeOH tend to lose their characteristic toughness. Similar trends as reported above, were observed.

Table 3-2 The mechanical properties of the degummed silk fibers and treated silk fibers* at 65% RH and 20ºC.

	Tenacity (gf/den)	**Toughness (gf/den)**	**Strain at break (%)**	**Modulus (GPa)**	**Toughness (gf/den)**
degummed silk	3.83±0.70	0.56±0.23	23.04±5.89	2.04±0.43	0.56±0.23
10%(w/w)	3.33±0.57	0.35±0.086	17.99±2.89	2.25±0.52	0.35±0.086
25% (w/w)	3.89±0.60	0.45±0.11	18.68±1.81	2.50±0.37	0.45±0.11
50% (w/w)	4.13±1.28	0.44±0.24	16.69±7.24	3.77±2.44	0.44±0.24
75% (w/w)	4.04±0.74	0.50±0.30	17.90±8.78	3.00±0.76	0.50±0.30
90% (w/w)	3.84±0.91	0.41±0.18	16.26±3.27	2.96±1.17	0.41±0.18

*Silk fibers treated in $Ca(NO_3)_2$ $4H_2O$/MeOH for 2 hours at room temperature were used. At least five replicates were tested.

3.3.7 Moisture absorption behavior of the treated silk fibers

Moisture absorption of degummed silk fibers and treated fibers in $Ca(NO_3)_2$ $4H_2O$/MeOH solutions were evaluated for a period of 24 hours at 20℃, 65% RH. The absorption of water is one of the important factors that causes changes in the size, shape, stiffness, and permeability of fibers. The amount of water in a specimen is generally expressed by moisture regain. Each water-absorbing material has a specific moisture regain, for example, cotton ~ 7%, wool ~14%, and silk ~ 11% at 20℃ 65% RH [108]. Silk has a regain intermediate between cotton and wool. The interaction between the water molecules and the fiber plays an important role in the absorption, there are some water absorbing groups that strongly attract water molecules. The protein fibers, like silk fibroin, contain water absorbing groups, amide groups (-NH-), in the main chain, and water can be hydrogen-bonded to this groups, as well as to other water-attracting groups, such as -OH, $-NH_3^+$, $-COO^-$, -CO・NH_2, in the side chains. The cotton that consists of cellulose has only hydroxyl groups as water absorbing group, while silk fibroin contains many water absorbing groups as shown above. This is a reason why moisture regain of silk is higher than that of cotton. In addition, physical structure of fibers also affects the moisture regain. In crystalline regions, the fiber molecules are closely packed together in a regular pattern and form cross-links between the molecules like hydrogen-bondings. Thus, it would not be easy for water molecules to penetrate into a crystalline region, and for absorption to take place. Silk has higher crystallinity (~70%) than wool (~40%), thus, less amorphous region leads to the smaller moisture regain than wool. In addition, the sericin, which binds the two fibroin

filaments of a silk fiber, has been reported to have a high regain and the degumming causes a reduction in regain at 65% RH from 10.65 to 9.9% [109].

The results are shown in Figure 3-17. The moisture regain (MR) of each sample was calculated by following equation:

MR(%)=(mass of absorbed water) g /(mass of dry fiber) g

As a result of moisture absorbing test, MR (%) of silk fibers treated in 50% (w/w) solution at 65℃, which was most severe condition, and in 50% (w/w) solution at room temperature showed higher values than that of the degummed silk fibers after 4 hours, while MR (%) of these two treated fibers in turn decreased and became smaller than that of the degummed silk fibers after equilibrium was reached. These results suggest us that these fibers initially could absorb more water due to large amorphous area as a result of decrystallization, however, they could not hold water for long time because the number of water absorbing groups were limited and water molecules tend to bond loosely with the fibers. In consequence, the absorbed water was easily evaporated. On the other hand, other fibers treated in 10% (w/w), 25% (w/w), 75% (w/w), and 90% (w/w) solutions at room temperature showed almost same or somewhat higher MR(%) values than that of the degummed silk. The moisture regain is a useful parameter on the degree of crystallinity. The obtained results would show that each sample has specific moisture absorbing behavior and support the FTIR and X-ray results that most effective decrystallization occurs for the treatments in 50% (w/w) solution.

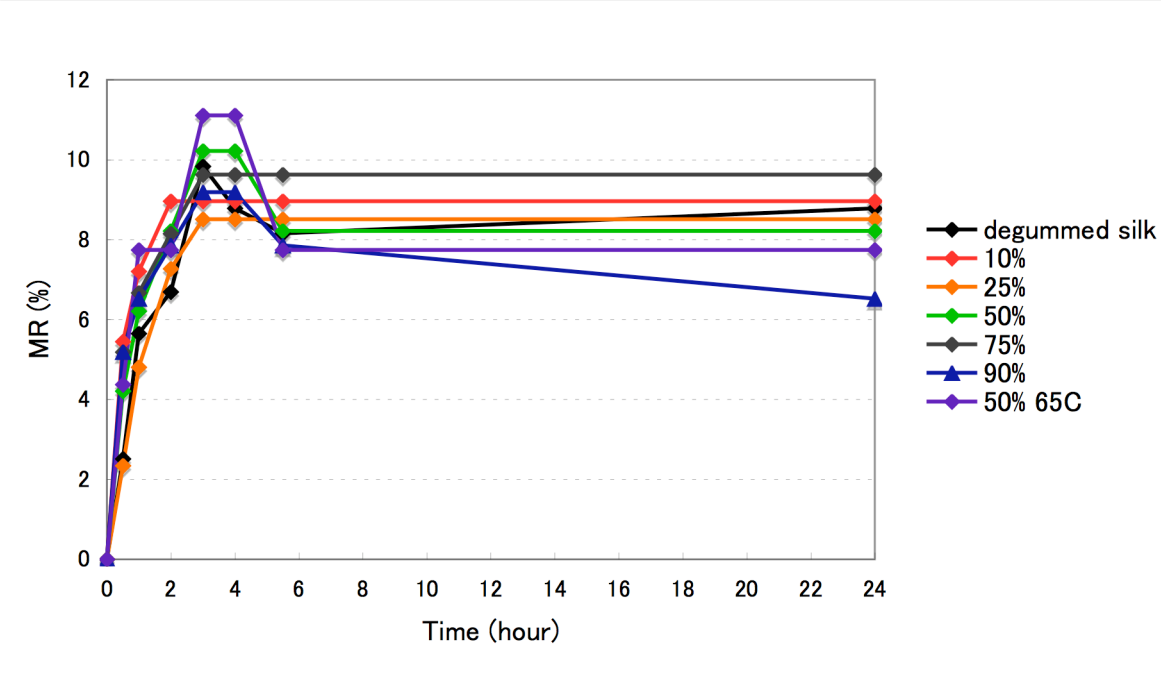

Figure 3-17 Moisture absorption of degummed silk fibers and various treated silk fibers.

3.3.8 Surface morphology of treated silk fibers

Figure 3-18 show surface SEM images of the degummed silk fibers and the treated silk fibers in 50% (w/w) $Ca(NO_3)_2$ $4H_2O$/MeOH at 65℃. The degummed silk fibers exhibited relatively uniform diameter with smooth surface (Figure 3-18 (a)). On the other hand, Figure 3-18 (b) clearly shows that the fibers treated in 50% (w/w) $Ca(NO_3)_2$ $4H_2O$/MeOH dissolved partially. As the increase in solution concentration of $Ca(NO_3)_2$ $4H_2O$/MeOH, the silk fibers seemed gradually to dissolve from their outside, resulting in the reduction in the diameter. The cracking of the fiber surface was also observed for the fibers treated in higher concentration solutions (Figure 3-18 (c)). The fibers treated in 50% (w/w) at 65℃ visibly looked different from the degummed silk fibers and other treated fibers. These fibers were easily broken by tweezers. We thought that the solvent easily penetrated inside of the fibers and caused the severe decrystallization both outside and inside under this condition, as a result, the fibers started to dissolve and stuck each other. The tensile properties in previous section demonstrated that the flexibility was lost while stiffness increased for these fibers. However, how the decrystallization proceeds has been still unclear and further morphology study in detail is needed for future work.

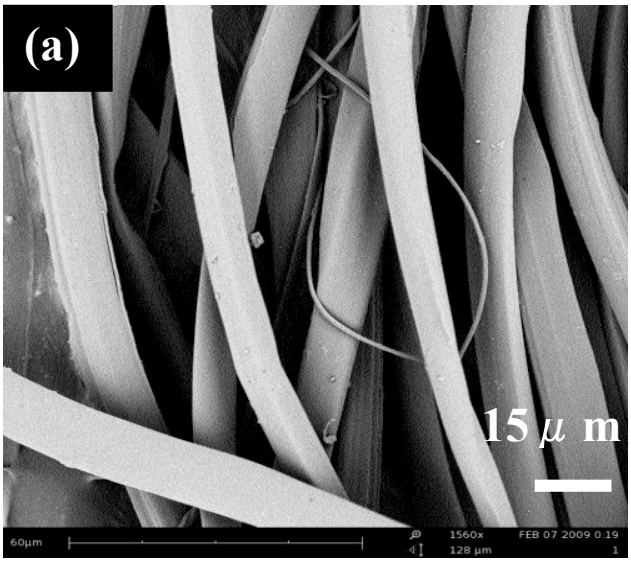

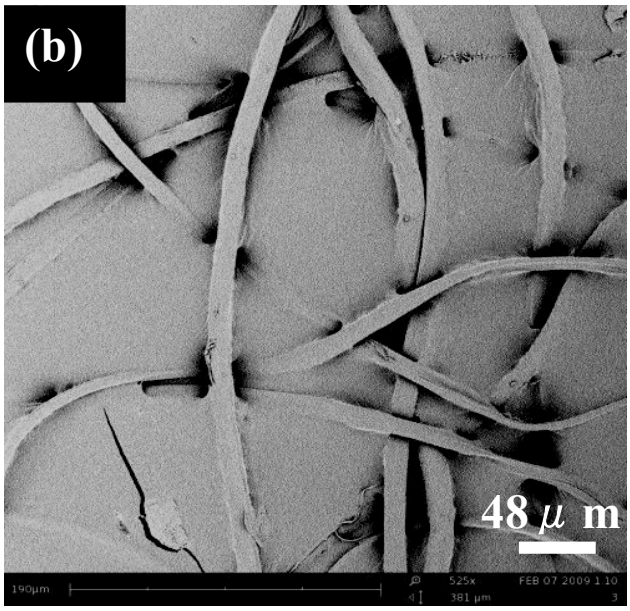

Figure 3-18 SEM image of fiber surface;(a) degummed silk fibers and (b) treated silk in 50% (w/w) $Ca(NO_3)_2$ $4H_2O$/MeOH at 65℃.

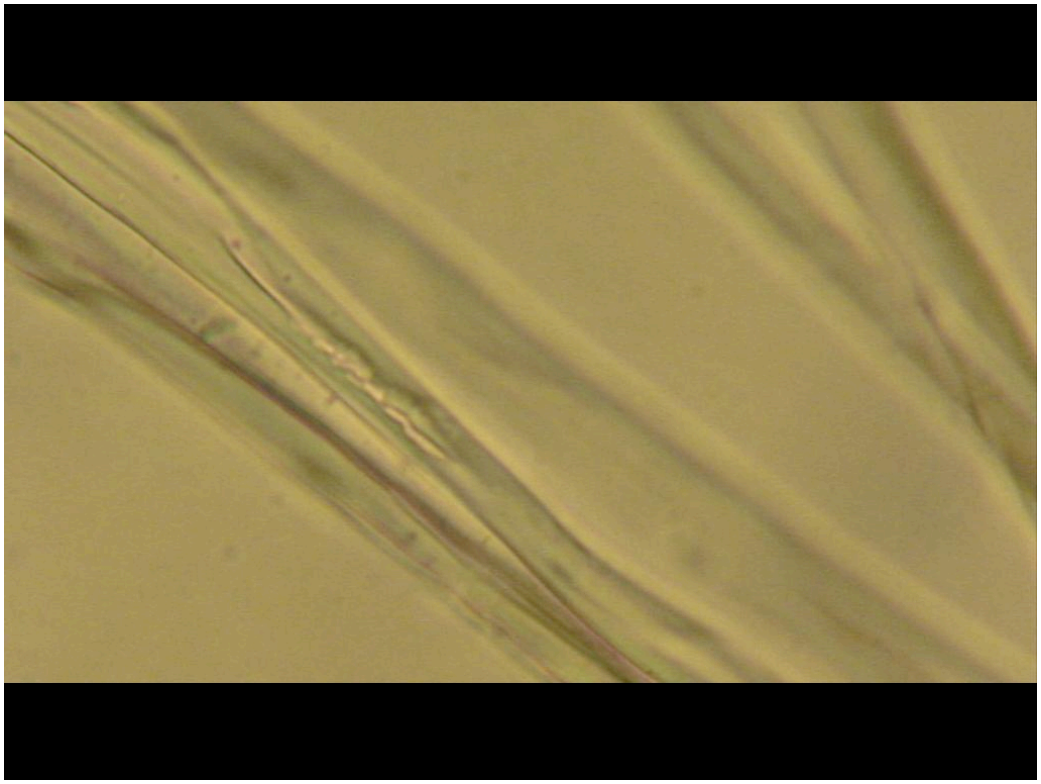

Figure 3-18 (c) Optical microscope image of the treated fibers in 75% (w/w) $Ca(NO_3)_2$ $4H_2O$/MeOH for 2 h at room temperature (x10).

4. HEMOSTATIC PROPERTIES OF SILK FIBERS

4.1 Introduction

As described in the previous chapter, silk has many expected biotechnological and biomedical applications, including surgical sutures [35, 41], substrate for cell culture [35, 37], controlled drug-delivery carriers [35, 45], and scaffolds for tissue engineering [35, 36]. However, there are only limited publications on the potential utility for wound dressing and hemostatic applications of the silk. Currently, wound dressings based on chitosan (HemCon®; HemCon Medical Technologies, Inc.), collagen (ActCel Hemostatic Gauze™; ActSys Medical, Inc.), cellulose (Surgicel®; Ethicon, Inc.), or potato starch (TraumaDEX®, Medafor, Inc.) are commercially available. We consider that silk is one of the promising biomaterials because of its biodegradability and great mechanical strength in wet condition. In this chapter, blood coagulation test was carried out to investigate the potential application of silk as hemostatic wound dressing.

4.2 Experimental

4.2.1 Materials

The same silk fibers as in Chapter 3 (Section 3.2.1) were also used here. All other chemicals used in this study were purchased from Fisher Scientific or Aldrich Chemicals and used without further purification.

4.2.2 Preparation of $Ca(NO_3)_2$ $4H_2O$/MeOH solution

$Ca(NO_3)_2$ $4H_2O$/MeOH solution of 10 %, 25%, 50%, 75%, 90% (w/w) were prepared by following the method of 3.2.2

4.2.3 Treatment of silk fibers in $Ca(NO_3)_2$ $4H_2O$/MeOH

The degummed silk fibers were immersed in 50% (w/w) $Ca(NO_3)_2$ $4H_2O$/MeOH solutions for 2 hours at 65℃ in oil bath. After 2 hours, the fibers were removed from the solution and rinsed in deionized water for 15 minutes and towel-dried.

4.2.4 Blood coagulation tests

Venous blood from a donor pig that was stabilized with heparin was obtained from College of Veterinary Medicine, NC State University. A total of 1mL of blood was transferred to each glass tube (10 x 75mm) and it was preincubated for 5 minutes in a water bath at 37ºC in water bath. The degummed silk fibers and the treated silk fibers in 50% (w/w) $Ca(NO_3)_2$ $4H_2O$/MeOH at 65℃ were divided into two specimens, respectively. One specimen of 0.01g was soaked in phosphate buffered saline (PBS, pH 7.0) for 30 minutes to be wet, and the other specimen of 0.01g was dried in vacuum oven before the test. The total four sets of specimens were put into the blood tubes, and the tubes were placed and incubated in the water bath at 37ºC until the blood was separated into two phases, supernatant and red blood cell aggregation. The tube was checked every 30 seconds until the blood sedimentation was completed at almost a 1:1 ratio of two phases. The time of blood sedimentation was recorded for each sample. At least two replicates were conducted. After

1.5 hours, all tests were stopped and the fibers were taken out from the blood pool. The samples were captured by digital camera at predetermined time intervals. The morphology of red blood cells was examined by Nikon Labophot2-POL equipped with COOLPIX digital camera. A drop from the phase containing red blood cells was placed on a glass plate and covered with a glass cover. The 10x and 40x lenses were used.

4.2.5 Hydrophobic treatment (SDS-modification)

Both the degummed silk fibers and the treated silk fibers in $Ca(NO_3)_2$ $4H_2O$/MeOH solution were soaked into 5% (w/w) aqueous acetic acid solution at room temperature for 30 minutes. The fibers were removed and washed gently with deionized water for 5 minutes in order to protonate any amino groups. Then, the two sets of fibers were soaked in a 1% (w/w) solution of sodium dodecyl sulfate (SDS) for 30 minutes for the purpose of formation of hydrophobic salts of the SDS with the silk. Finally, the fibers were rinsed for 5 minutes in deionized water again to remove excess SDS.

4.3 Results and Discussion

4.3.1 Blood coagulation tests

The blood coagulation test was conducted by measuring the time of erythrocyte sedimentation in anti-coagulated blood that has previously been reported by Yamazaki et al. [16]. The degummed silk fibers and the treated silk fibers were added into the blood in conventional glass tubes (7.5 x 10 mm) and the blood sedimentation time when the supernatant and erythrocyte agglutination were separated as equal phases at 1:1 were

recorded. As summarized in Table 4-1, the clear blood sedimentation was observed more or less for every sample with dry and wet conditions within up to 1.5 hours. First, the degummed silk fibers exhibited the faster blood sedimentation rate at 10.0 mm/hour with dried condition, and 16.0 mm/hour with wet condition (Figure 4-1). On the other hand, the treated fibers in 50% (w/w) $Ca(NO_3)_2$ $4H_2O$/MeOH at 65℃, which was a most severe condition, showed lower blood sedimentation rate at 5.33 mm/hour with dried condition, and 7.78 mm/hour with wet condition (Figure 4-2). This experiment clearly shows that degummed silk fibers cause faster erythrocyte aggregation than the treated fibers. As mentioned in Chapter 2, serum protein, fibrinogen, is likely to bind with silk fibroin fibers on more hydrophobic sites through strong hydrophobic interactions and help make fibrin crosslinking. Santin et al. [51] reported that when silk fibers were treated with 9.3M LiBr for 3 hours, the destabilizing ions disrupted the hydrogen bonding and induced the transition of the silk fibroin from crystalline β -sheet structure (silk II) to a random coil conformation (silk I), causing less binding of the serum proteins with the more hydrophilic regenerated fibroin films. In the same way, the treated silk fibers with $Ca(NO_3)_2$ $4H_2O$/MeOH solutions started to be decrystalized partially and resultant more hydrophilic surfaces of the fibers lead to less binding with the serum protein, compared with the original degummed silk fibers. This would be a reason why the blood sedimentation rate became slower for the treated fibers.

Table 4-1 Blood sedimentation of various silk fibers in 1mL of anti-coagulant blood after 1 hour.

	Degummed silk (mm)	Treated silk* (mm)
Dry	10.0	5.33
Wet	16.0	7.78

*Silk fibers treated in 50% (w/w) $Ca(NO_3)_2$ $4H_2O$/MeOH for 2 hours at 65℃ were used.

Table 4-2 Blood sedimentation of various silk fibers with hydrophobic treatment in 1mL of anti-coagulant blood after 1 hour.

	Degummed silk (mm)	Treated silk*(mm)
Non-modified	7.33	2.52
SDS-modified	5.66	2.40

*Silk fibers treated in 50% (w/w) $Ca(NO_3)_2$ $4H_2O$/MeOH for 2 hours at 65℃ were used.

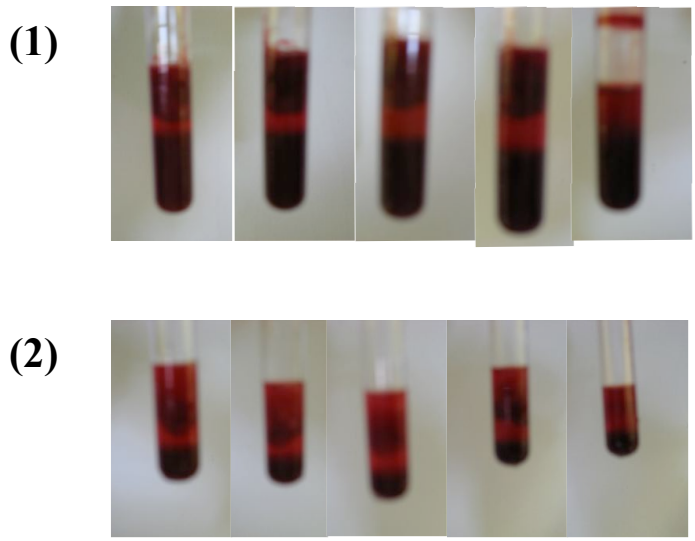

Figure 4-1 Blood sedimentation after immersing of degummed silk fibers of dry condition (1), and wet condition (2) at 37 ºC: (a) 10 min, (b) 20 min, (c) 30 min, (d) 60 min, (e) 60 min after removing silk.

(1)

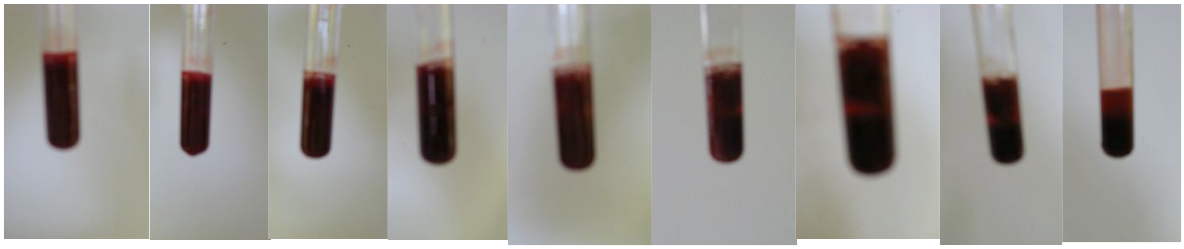

(2)

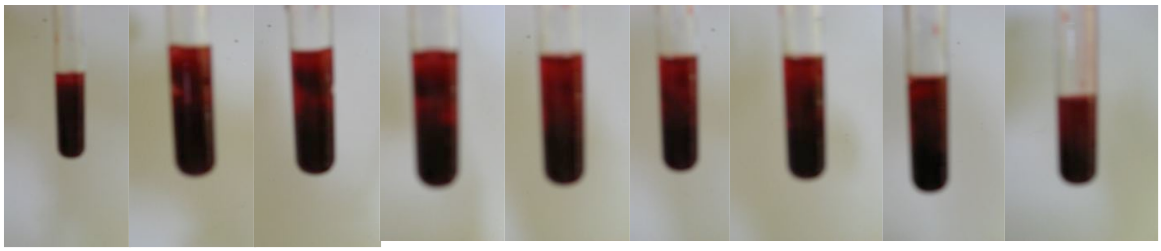

(a) (b) (c) (d) (e) (f) (g) (h) (i)

Figure 4-2 Blood sedimentation after immersing of treated silk fibers of dry condition (1), and wet condition (2) at 37℃: (a) 5 min, (b) 10 min, (c) 20 min, (d) 30 min, (e) 40 min, (f) 50 min, (g) 60 min, (h) 90 min, (i) 90 min after removing silk.

4.3.2 Effect of hydrophobic treatment

Santin et al. also reported that the formaldehyde-treated silk fibers dramatically inhibited fibrin(ogen) binding to the silk fibroin fibers and only poorly bound polymerized clots were observed in a few non-representative areas [51]. Based on this previously reported result and the obtained result in our experiment, the hydrophobicity of silk fibers surface plays an important role in binding serum protein with the fibers.

In order to confirm that the hydrophobicity of the silk fibers is a key factor in binding of serum proteins, the degummed silk fibers modified with a hydrophobic treatment by SDS were investigated regarding their effect on blood sedimentation. The results are summarized in Table 4-2. In contrast to our expectations, the SDS-modified degummed silk fibers did not bring about obvious enhancements on the blood sedimentation rate, in fact, the blood sedimentation rate for the SDS-modified degummed fibers was lower by 23% compared with the case of un-SDS modified degummed silk fibers as shown in Figure 4-3.

The fibers treated in $Ca(NO_3)_2\ 4H_2O$/MeOH were exposed to the hydrophobic modification in the same way. As mentioned above, the treated fibers showed much less blood sedimentation due to the loss of β -sheet crystalline structure and its hydrophobicity through decrystallization. As well as the degummed silk fibers, the blood sedimentation rate for the treated fibers was not dramatically improved even after hydrophobic treatment was done as shown in Figure 4-4. This would tell us that not only hydrophobicity but also some specific chemical structure of silk fibroin fibers might be necessary for binding serum proteins (Figure 4-5). Also, we assume that the hydrophobic treatment we did was not sufficient for the hydrophobic chains of SDS to be successfully placed on the surface of silk

fibers through the modification. Another experiment for hydrophobic modification would be helpful to confirm that the serum proteins bind to more hydrophobic site on the silk fiber through the hydrophobic interaction.

Since there were no obvious blood clot formations observed on the fiber surface during all experiments, the red blood cell morphology in the sedimentation phase was checked. After the blood sedimentation test was stopped, a drop was taken from sedimentation phase and the red blood cell morphology was examined (x 10) by an optical microscope as shown in Figure 4-6. There were few red blood cell coagulation observed in anti-coagulant blood without the silk fibers after incubating for 1.5 hours at 37℃ (Figure 4-6 (e)). On the other hand, partly aggregated red blood cells were observed in the sedimentation phase when the degummed silk fibers and the treated silk fibers were added to the blood. In addition, SDS-modified fibers might cause slightly more red blood cell aggregation, compared with un-modified fibers in Figure 4-6 (c,d), indicating that hydrophobic treatment approach would be useful to improve rapid clotting ability. Finally, the immersed silk fibers in the anti-coagulant blood were taken out and morphology was observed by optical microscope. As shown in Figure 4-7, the red blood cells were bound by the fibers.

At this point, the detail mechanism of how the silk fibers interact with blood proteins has not been clarified. More studies will be needed to determine how decrystallization of the silk fibers affect the blood clotting, otherwise it is not useful for binding serum protein. The blood used in this study contained heparin, which is widely used as an anticoagulant, preventing the formation of clots and extension of existing clots within the blood. Heparin binds to the enzyme inhibitor antithrombin (AT), which inactivates thrombin and other

proteases involved in blood clotting [110, 111]. Therefore, our experiments do not exactly replicate the actual interaction between blood proteins and silk fibers. Another experiment using raw blood that does not contain any anticoagulants must be needed. Nevertheless, the obtained results suggest that the silk fibers somewhat trigger the red blood cell sedimentation.

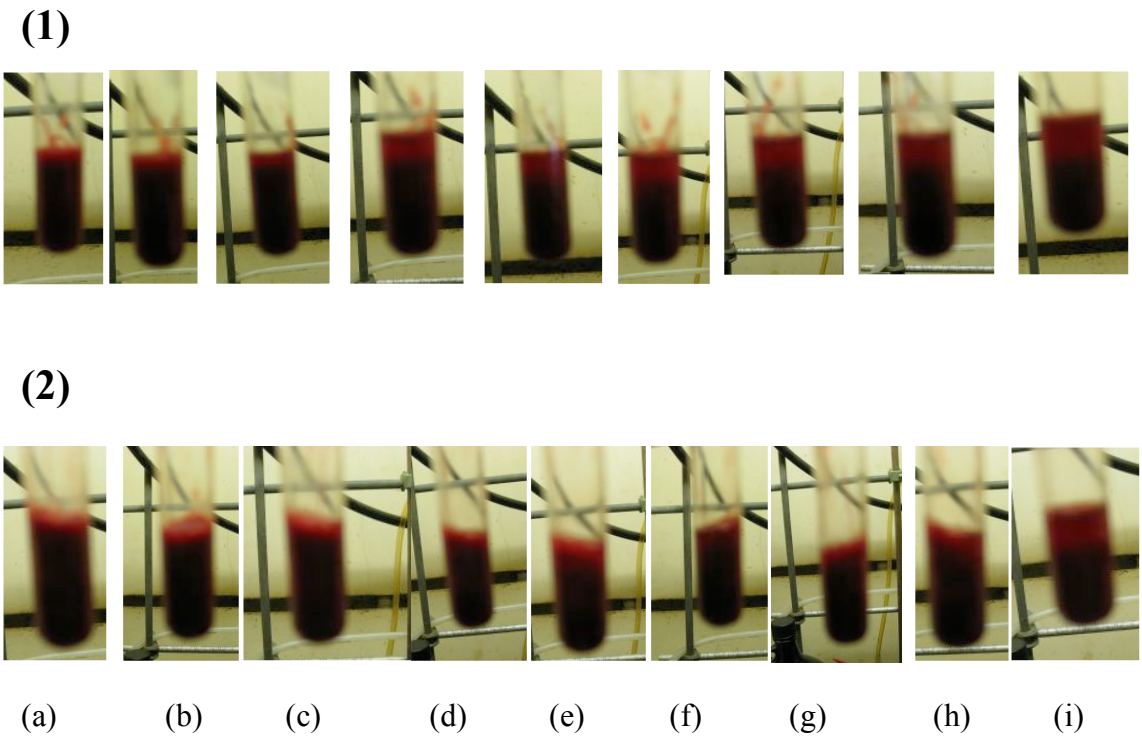

Figure 4-3 Blood sedimentation after immersing of degummed silk fibers (1), and SDS-modified degummed silk fibers (2) at 37℃: (a) 5 min, (b) 10 min, (c) 20 min, (d) 30 min, (e) 40 min, (f) 50 min, (g) 60 min, (h) 90 min, (i) 90min after removing silk

(1)

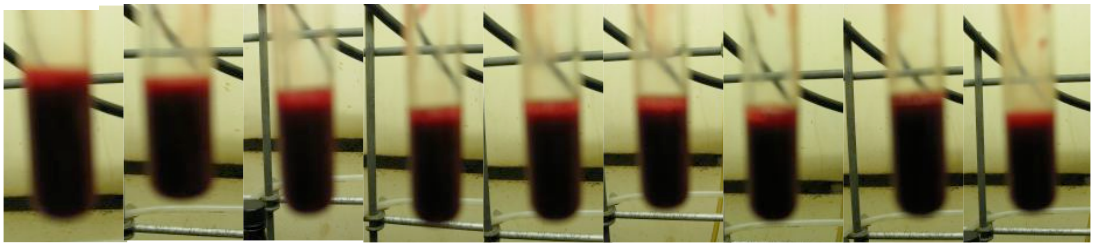

(2)

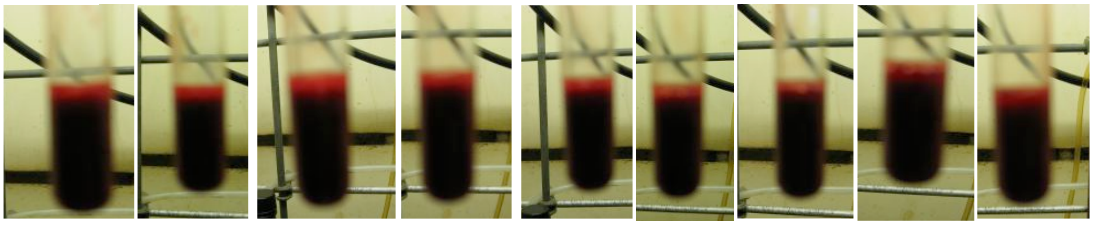

(a) (b) (c) (d) (e) (f) (g) (h) (i)

Figure 4-4 Blood sedimentation after immersing of the treated silk fibers (1), and SDS-modified treated fibers (2) at 37℃: (a) 5 min, (b) 10 min, (c) 20 min, (d) 30 min, (e) 40 min, (f) 50 min, (g) 60 min, (h) 90 min, (i) 90 min after removing silk

(1) **(2)**

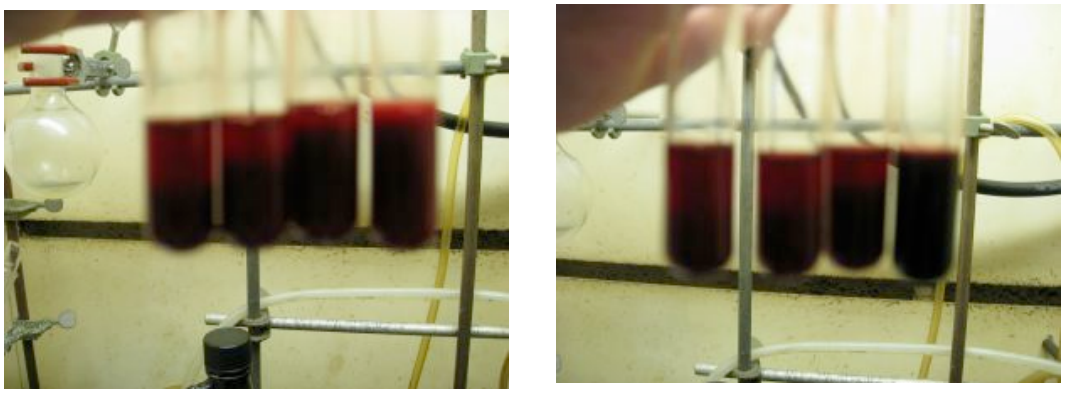

Figure 4-5 Blood sedimentation after stopping the experiments; 90 minutes later (1), and 24 hours later (2); From left, degummed silk, SDS-modified degummed silk, treated silk, SDS-modified treated silk in each picture.

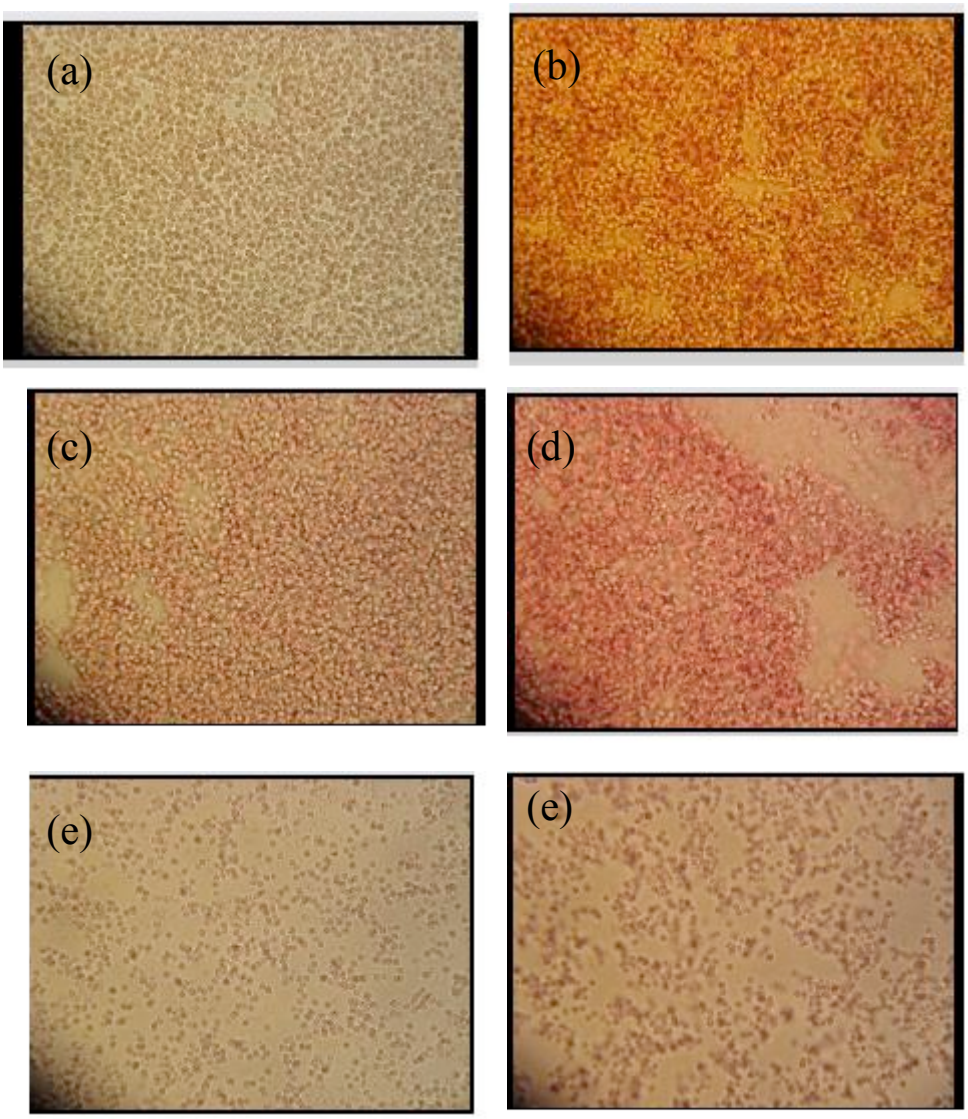

Figure 4-6 Optical microscope images (x10) of red blood cells after 1.5 hour-sedimentation; (a) degummed silk fibers, (b) treated silk fibers*,
(c) SDS-modified degummed silk fibers, (d) SDS-modified treated silk fibers*,
(e) anti-coagulated blood without fibers.

*Treated silk fibers in 50% (w/w) $Ca(NO_3)_2$ $4H_2O$/MeOH for 2hours at 65℃were used.

(a)

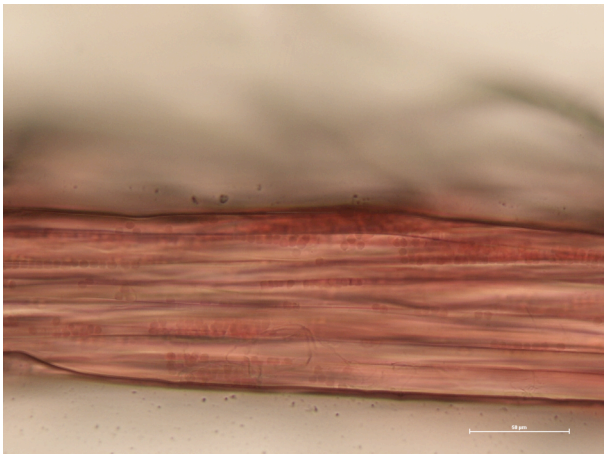

(b)

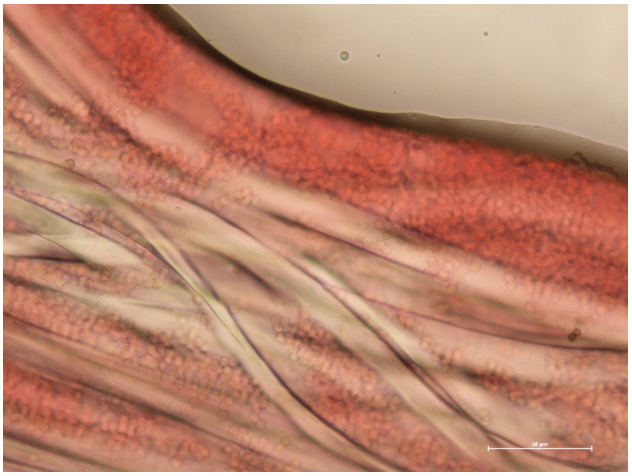

Figure 4-7 Optical microscope images of silk fibers immersing in anti-coagulant blood for 1.5 hours (x40); (a) degummed silk fibers, and (b) treated fibers in 50%(w/w) $Ca(NO_3)_2$ $4H_2O$/MeOH for 2 hours at 65℃. Red blood cells are seen bound to the fibers. Scale bar is 50 μ m.

5. CONCLUSIONS AND RECOMMENDATION FOR FUTURE WORK

The original silk fibers were decrystallized with two kinds of neutral salt-water alcohol systems. The chemical structure of the treated silk fibers was characterized by FTIR and X-ray to investigate the degree of decrystallization. Any obvious shifts of specific peaks that correspond with conformational transition from β -sheet to random coil, amide I, II, III, were not observed in FTIR spectra, even though there was somewhat change in peak intensity. We could not exactly confirm whether decrystallization was achieved or not through FTIR data. Since FTIR spectra are usually considered s a qualitative analysis, other quantitative techniques must be needed to determine the amount of crystalline structure. In this study FTIR-ATR method was used, but spectra using KBr pellet will be give us more accurate data about the crystallinity.

X-ray diffraction revealed that $Ca(NO_3)_2$ $4H_2O$/MeOH and $CaCl_2$/MeOH caused largest decrystallization under the condition of 50% (w/w) and 65℃. Through controlling two parameters, i.e., concentration of the solutions and environmental temperature, this condition was determined to be most severe treatment for decrystallization. Above this concentration and temperature, the fibers were perfectly dissolved. Also, the fibers were not sufficiently decrystallized at room temperature for every concentration. The detail mechanism how the silk fibers were decrystallized in these systems has still been unclear and further study is needed.

Average crystal sizes of the silk fibers were estimated based on the results of X-ray diffraction. Only the fibers treated in 50% (w/w) $Ca(NO_3)_2$ $4H_2O$/MeOH at room

temperature and at 65℃ exhibited obvious decrease in the crystal size than that of the degummed silk fibers. On the other hand, $Ca(NO_3)_2$ $4H_2O$/EtOH did not bring about any changes in crystal size of the fibers, indicating less decrystallizing ability of this solvent. Moreover, $CaCl_2$/MeOH caused the recognizable decrease in crystal size under the condition of 50% (w/w) concentration at 65℃, although the effect was still lower than the $Ca(NO_3)_2$ $4H_2O$/MeOH.

The mechanical properties of the treated fibers were tested by tensile tests. The results showed that strength and elongation at break gradually increase with the solvent concentration up to 50% (w/w) then decrease while modulus gradually increases as the concentration of the solution was increased, suggesting that the fibers lost their flexibility and turned to be more brittle. This could support X-ray results that minimum crystallinity was observed at 50% (w/w). At this point, we cannot explain why degree of decrystallization was lowest in 50% (w/w) solution, not 75% (w/w) or 90% (w/w) solution, and further work on detail morphology study of the treated silk fibers should be needed.

Moisture regain curve of the fibers could be another way to measure crystallinity and information about their moisture absorption behavior. As the decrystallization proceeds, the fibers initially absorbed more water, however, the amount of absorbed water was small after equilibrium was reached. We consider these results that the increased amorphous region due to the decrystallization brought about the increase in amount of absorbed water initially, on the other hand, they cannot hold water for long time because of limited number of amide groups and hydroxyl groups that bond water molecules tightly through hydrogen bonds. This is somewhat evidence that the degree of crystallinity was decreased after the treatments.

Both the degummed silk and the treated silk caused somewhat red blood cell aggregation. Since clear blood clots were not formed on the fiber during the blood coagulation tests, the red blood cell aggregation ability was measured by microscopic observations of sedimentation phase in the blood after the test. The blood coagulation test revealed that the treated silk fibers lead to less red blood cell coagulation than the original degummed silk fibers due to their less hydrophobicity. Since hydrophobic modification of the silk fibers by SDS did not bring about any obvious improvement on the red blood cell aggregation, we could not conclude that the hydrophobic modification could be a trigger of red blood cell aggregation in this research. Some replicates or other hydrophobic modification techniques as well as other evaluation methods for the blood coagulation are needed to reveal how the silk fibers interact with the blood proteins. In addition, the anti-coagulant blood stabilized by heparin citrate was used in this research, but the blood coagulation test using fresh blood that is not stabilized will give us more accurate data to investigate the potential of the silk fibers as hemostatic wound dressings.

In conclusion, this study focused on the potential ability of *Bombyx mori* silk fibroin as hemostatic wound dressing. We first consider that decrystallization of silk fibers must be needed in order to improve or enhance water absorbability or biodegradability of the silk because silk fibroin has strong crystalline structure and are inert to reactions. However, we have not obtained sufficient evidence to clarify the decrystallized silk fibers would be more useful for blood coagulation at this point. Other methods to measure the amount of red blood cell aggregation quantitatively would be needed in future study as well as detail interaction between the silk and blood proteins.

6. REFERENCES

[1] Hanson SR. Encyclopedia of Biomaterials and Biomedical Engineering. New York: Dekker Pub 2004: 144-154.

[2] Kozen BG, Kircher SJ, Henao J, Godinez FS, Johnson AS. An Alternative Hemostatic Dressing: Comparison of CELOX, HemCon, and QuikClot. Acad Emerg Med 2008; 15 (1): 74-81.

[3] Champion HR, Bellamy RF, Roberts CP, Leppaniemi A. A profile of combat injury. J Trauma 2003; 54: S13-S19.

[4] Dickinson E. Clotting Agents. Law Officer Magazine 2008; 4(3).

[5] Sauaia A, Moore FA, Moore EE et al. Epidemiology of trauma deaths: a reassessment. J Trauma 1995; 38:185–93.

[6] Palm MD, Altman JS. Topical hemostatic agents: A review. Dermatologic Surgery 2008; 34(4): 431-445.

[7] Hwang JJ, Stupp SI. Poly(amino acid) bioadhesives for tissue repair. J Biomater Sci Polymer Edn 2000; 11: 1023-1038.

[8] Alam HB, Chen Z, Jaskille A et al. Application of a zeolite hemostatic agent achieves 100% survival in a lethal model of complex groin injury in swine. J Trauma 2004; 56: 974-983.

[9] Acheson EM, Kheirabadi BS, Deguzman R, Dick EJ Jr, Holcomb JB. Comparison of hemorrhagic control agents applied to lethal extremity arterial hemorrhage in swine. J Trauma 2005; 59: 865-875.

[10] Alam HB, Uy GB, Miller D et al. Comparative analysis of hemostatic agents in a

swine model of lethal groin injury. J Trauma 2003; 54:1077-1082.

[11] Pusateri AE, Delgado AV, Dick EJ Jr et al. Application of granular mineral-based hemostatic agent (QuikClot) to reduce blood loss after grade V liver injury in swine. J Trauma 2004; 57: 555-562.

[12] Wright JK, Kalns J, Wolf EA et al. Thermal injury resulting from application of a granular mineral hemostatic agent. J Trauma 2004; 57: 224-230.

[13] Whang HS, Kirsch W, Zhu YH, Yang CZ, and Hudson SM. Hemostatic agents derived from chitin and chitosan. J Macromol Sci Polym Rev 2005; 45(4): 309-323.

[14] Alam HB, Burris D, DaCorta JA, Rhee P. Hemorrhage control in the battlefield: role of new hemostatic agents. Mil Med 2005; 170(1): 63–69.

[15] Gobin AS, Froude VE, Mathur AB. Structural and mechanical characteristics of silk fibroin and chitosan blend scaffolds for tissue regeneration. J Biomed Mater Res 2005; 74A(3): 465–473.

[16] Yamazaki M. The Chemical Modification of Chitosan Films for Improved Hemostatic and Bioadhesive Properties, Ph. D dissertation at North Carolina State University (2007)

[17] Barrera DA, Zylstra E, Lansbury PT, Langer R. Sysnthesis and RGD peptide modification of a new biodegradable copolymer: poly(lactic acid-*co*-lysin). J Am Chem Soc 1993; 115: 11010-11011.

[18] Hu Y, Winn SR, Krajbich I, Hollinger JO. Porous polymer scaffolds surface-modified with arginine-glycine-aspartic acid enhance bone cell attachment and differentiation *in vitro*. J Biomed Mater Res 2003; 64A: 583-590.

[19] Moon SI, Lee CW, Miyamoto M, Kimura Y. Melt polycondensation of L-lactic acid with Sn(II) catalysts activated by various proton acids: a direct manufacturing route to high molecular weight poly(L-lactic acid). J Polym Sci Part A 2000; 38: 1673-1679.

[20] Shinoda H, Asou Y, Suetsugu A, Tanaka K. Synthesis and characterization of amphiphilic biodegradable copolymer, poly(aspartic acid-co-lactic acid). Macromol Biosci 2003; 3: 34-43.

[21] Takahashi A, Kita R, Kaibara M. Effects of thermal annealing of segmentated polyurethane on surface properties, structure and antithrombogenecity. J Mater Med 2002; 13: 259-264.

[22] Wang XH, Li DP, Wang WJ, Feng QL, Cui FZ, Xu YX, Song XH, Werf M. Crosslinked collagen/chitosan matrix for artificial livers. Biomaterials 2003; 24: 3213-3220.

[23] Wang X, Yan Y, Zhang R. A comparison of chitosan and collagen sponges as hemostatic dressings. J Bioact Compat Polym 2006; 21: 39-53.

[24] Hirano S, Noishiki Y. The blood compatibility of chitosan and *N*-acylchitosans. J Biomed Mater Res 1985; 19: 413-417.

[25] Rao SB, Sharma CP. Use of chitosan as a biomaterial: Studies on its safety and hemostatic potential. J Biomed Mater Res 1997; 34: 21-28.

[26] Klokkevold PR, Fukuyama H, Sung EC, Bertolami CN. The effect of chitosan (poly-*N*-acetyl glucosamine) on lingual hemostasis in heparinized rabbits. J Oral Maxillofac Surg 1999; 57: 49-52.

[27] Ha, Sung-Won, Structural Study of *Bombyx mori* Silk Fibroin during Processing for Regeneration, Ph. D dissertation at North Carolina State University (2004)

[28] Sofia S, McCarthy MB, Gronowicz G, Kaplan DL. Functionalized Silk based Biomaterials for Bone Formation. Biomed. Mater. Res 2001; 54: 139-148.

[29] Bunning TJ, Jiang H, Wade Adams W, Crane RL, Farmer B, Kaplan DL. Applications of Silk. Materials Science and Biotechnology, ACS Symp Series 544 Washington D.C. 1994; 353-358.

[30] Liu Y, Zhang X, Liu H, Yu T, Deng J. Immobilization of Glucose Oxidase onto the Blend Membrane of poly(vinyl alcohol) and Regenerated Silk Fibroin: Morphology and Application to Glucose Biosensor. J Biotechnol 1996; 46: 131-138.

[31] Tsukada M, Freddi G, Minoura N, Allara G. Preparation and Application of Porous Silk Fibroin Materials. J Appl Polym Sci 1994; 54: 507-514.

[32] Gil ES. Stimuli-Responsive Protein-Based Hydrogels by Utilizing β-Sheet Conformation of Silk Fibroin as Cross-Links. Ph.D dissertation at North Carolina State University 2004

[33] Nazarov R, Jin H, Kaplan D. Porous 3-D Scaffolds from Regenerated Silk Fibroin. Biomacromolecules 2004; 5: 718-726.

[34] Gotoh Y, Tsukada M, Minoura N, Imai Y. Synthesis of poly(ethylene glycol)-silk fibroin conjugates and surface interaction between L-929 cells and the conjugates. Biomaterials 1997; 18: 267-271.

[35] Minoura N, Tsukada M, Nagura M. Fine Structure and Oxygen Permeability of Silk Fibroin Membrane Treated with Methanol. Polymer 1990; 31: 265- 269.

[36] Minoura N, Tsukada M, Nagura M. Physico-chemicapl roperties of silk fibroin membrane as a biomaterial. Biomaterials 1990; 11(6): 430-434.

[37] Chen J, Minoura N, Tanioka A. Transport of pharmaceuticals through silk fibroin membrane. Polymer 1994; 35: 2853–2856.

[38] Gu J, Yang X, Zhu H. Surface sulfonation of silk fibroin film by plasma treatment and in vitro antithrombogenicity study. Materials Science and Engineering: C 2002; 20: 199-202.

[39] Vonfraunhofer JA, Sichina WJ. Characterization of surgical suture materials using dynamic mechanical analysis. Biomaterials 1992; 13: 715-720.

[40] Padamwar MN, Pawar AP. Silk sericin and its applications: A review. J Scientific and Industrial Research 2004; 63: 323-329.

[41] Zhang YQ. Natural silk fibroin as a support for enzyme immobilization. Biotechnology Advances1998; 16: 961-971.

[42] Santin M, Motta A, Freddi G, Cannas M. *In vitro* evaluation of the inflammatory potential of the silk fibroin. J Biomedical Material Research Part A 1999; 46: 382-389.

[43] Rujiravanit R, Kruaykitanon S, Jamieson AM, Tokura S. Preparation of crosslinked chitosan/silk fibroin blend films for drug delivery system. Macromol Biosci 2003; 3: 604-611.

[44] Chen X, Li W, Shao Z, Zhong W, Yu T. Separation of alcohol–water mixture by pervaporation through a novel natural polymer blend membrane-chitosan/silk fibroin blend membrane. J Appl Polym Sci 1999; 73: 975-980.

[45] Matsumoto K, Uejima H, Iwasaki T, Sano Y. Studies on Regenerated Protein Fibers; III. Production of Regenerated Silk Fibroin Fiber by the Self- Dialyzing Wet Spinning Method. J Appl Polym Sci 1996; 60: 503-511.

[46] Liivak O, Blye A, Shah N, Jelinsky LW. A Microfabricated Wet-Spinning Apparatus to Spin Fibers of Silk Proteins; Structure-Property Correlations. Macromolecules 1998; 31: 2947-2951.

[47] Seidel A, Liivak O, Calve S, Adaska J, Ji G, Yang Z, Crubb D, Zax DB, Jelinsky LW. Regenerated Spider Silk; Processing, Properties, and Structure. Macromol 2000; 33: 775-780.

[48] Arai T, Freddi G, Innocenti R, Tsukada M. Biodegradation of *Bombyx mori* Silk Fibroin Fibers and Films. J Appl Polym Sci 2004; 91: 2383–2390.

[49] Seves A, Romano M, Maifreni T, Sora S, Ciferri O. The microbial degradation of silk: a laboratory investigation, International Biodeterioration and Biodegradation 1998;

42(4): 203-211.

[50] Minoura N, Aiba S, Gotoh Y, Tsukada M, Imai Y. Attachment and growth of cultured fibroblast cells on silk protein matrices. J Biomed Mater Res 1995; 29: 1215–1221.

[51] Santin M, Denyer SP, Lloyd AW, Motta A. Domain-Driven Binding of Fibrin(ogen) onto Silk Fibroin Biomaterials. J Bioactive and Compatible Polymers 2002; 17: 195-208.

[52] Motta A, Migliaresi C, Lloyd AW, Denyer SP, Santin M. Serum Protein Absorption on Silk Fibroin Fibers and Films: Surface Opsonization and Binding Strength. J Bioactive and Compatible Polymers 2002; 17: 23–35.

[53] Earland C, Raven DJ. A New Solvent for Silk. Nature 1954; 174: 461.

[54] Tsukada M, Gotoh Y, Nagura M, Minoura N, Kasai N, Freddi G. Structural Changes of Silk Fibroin Membranes Induced by Immersion in Methanol Aqueous Solutions. J Polym Sci B: Polym Phys 1994; 32: 961-968.

[55] Chen CC, Riou S, Hsu SL, Stidham HD. Characterization of Silk Crystallization Behavior on Highly Oriented Substrates. Langmuir 1996; 12: 1035-1039.

[56] Sagar AJ, Narasinga Rao MS, Pandit MW. Properties of Silk Proteins Extracted in Saturated Lithium Thiocyanate Solution. Ind. J. Biochem. Biophys 1978; 15: 59-61.

[57] Bhat NV, Ahirrao SM. Investigation of the Structure of Silk Film Regenerated with Lithium Thiocyanate Solution. J Polym Sci: Polym Chem Ed 1983; 21(5): 1273-1280.

[58] Soong HK, Kenyon KR. Adverse reactions to virgin silk sutures in cataract surgery. Ophthalmology 1984; 91: 479–483.

[59] Lotz B, Cesari FC. The Chemical and the Crystalline Structures of *Bombyx mori* Silk Fibroin. Biochimie 1979; 61: 205-214.

[60] Magoshi J, Magoshi Y, Nakamura S. Crystallization, Liquid Crystal, and Fiber Formation of Silk Fibroin. J Appl Polym Sci: Appl Polym Symp 1985; 41: 187–204.

[61] Lotz B, Cesari FC. The Chemical Structure and the Crystalline Structures of *Bombyx mori* Silk Fibroin, Biochemie 1979; 61:205–214.

[62] Franz G, Alban S. Structure-activity relationship of antithrom antithrombotic polysaccharide derivatives. Int J Biol Macromol 1995; 17: 311–314.

[63] Fraser RBD, MacRae TP. Chapter 13. Silks. In: *Conformation in Fibrous Proteins*; Academic Press: New York and London 1973; 293-343.

[64] Cantor EJ, Creel HS, Deguchi Y, Dougherty MJ, Kothakota S, Krejchi MT, Matsuki K, McGrath KP, Parkhe AD, Atkins EDT, Fournier MJ, Mason TL, Tirrell DA. In Vivo Synthesis and Structural Analysis of Alanylglycine-Rich Artificial Proteins. Mater Sci and Biotech: ACS sympo series 544, Washington D.C. 1994 : 98-103.

[65] Tanaka K, Inoue S, Mizuno S. Hydrophobic Interaction of P25, Containing Asn-linked Oligosaccharide Chains, with the H-L Complex of Silk Fibroin Produced by *Bombyx mori*. Insect Biochem Mol Biol 1999; 29: 269-276.

[66] Takahashi Y, Gehoh M, Yuzuriha K. Structure refinement and diffuse streak scattering of silk (*Bombyx mori*). Int J Biol Macromol 1999; 24(2-3): 127-138.

[67] Ha SW, Gracz HS. Tonelli AE, Hudson SM. Structural Study of Irregular Amino Acid Sequences in the Heavy Chain of Bombyx mori Silk Fibroin. Biomacromolecules 2005; 6(5): 2563-2569.

[68] Freddi G, Pessina G, Tsukada M. Swelling and dissolution of silk fibroin (Bombyx mori) in *N*-methyl morpholine *N*-oxide, Int J Biol Macromol 1999; 24(2-3): 251-263.

[69] Fraser RDB, MacRaeIn TP. Conformation in Fibrous Proteins and Related Synthetic Polypeptides. Academic Press, NY 1973: 293–343.

[70] Ha SW, Park YH, Hudson SM. Dissolution of Bombyx mori Silk Fibroin in the Calcium Nitrate Tetrahydrate-Methanol System and Aspects of Wet Spinning of Fibroin Solution. Biomacromolecules 2003; 4: 488-496.

[71] Asakura T, Watanabe T, Uchida A, Minagawa H. NMR of Silk Fibroin 2: ^{13}C NMR Study of the Chain Dynamics and Solution Structure of *Bombyx mori* Silk Fibroin. Macromolecules 1984; 17: 1075-1081.

[72] Tsukada M, Gotoh Y, Nagura M, Minoura N, Kasai N, Freddi G. Structural Changes of Silk Fibroin Membranes Induced by Immersion in Methanol Aqueous Solutions. J Polym Sci B: Polym Phys 1994; 32: 961-968.

[73] Lucas F, Shaw JTB, Smith SG. The silk fibroins. Adv Protein Chem 1958; 13: 107–242.

[74] Sagar AJ, Narasinga Rao MS, Pandit MW. Properties of Silk Proteins Extracted in Saturated Lithium Thiocyanate Solution. Ind J Biochem Biophys 1978; 15: 59-61.

[75] Sun Y, Shao Z, Ma M, Hu P, Liu Y, Yu T. Acrylic polymer-silk fibroin blend fibers. J Appl Polym Sci 1997; 65(5): 959–966.

[76] Sun Y, Shao Z, Hu P, Yu T. Hydrogen bonds in silk fibroin-poly (acrylonitrile-co-methyl acrylate) blends: FT-IR study. J Polym Sci B: Polym Phys 1997; 35(9): 1405-1414.

[77] Ajisawa A. Dissolution of Silk Fibroin with Calciumchloride/Ethanol aqueous solution. J Seric Sci Jpn 1998; 67: 91-94.

[78] Um IC, Kweon HY, Park YH, Hudson SM. Structural Characteristics and Properties of the Regenerated Silk Fibroin Prepared from Formic Acid. Int J Biol Macromol 2001; 29: 91-97.

[79] Nam J, Park YH. Morphology of Regenerated Silk Fibroin: Effects of Freezing Temperature, Alcohol Addition, and Molecular Weight. J Appl Polym Sci 2001; 81: 3008-3021.

[80] Liang CX, Hirabayashi K. Improvements of the physical properties of fibroin membranes with sodium alginate. J Appl Polym Sci 1992; 45(11):1937–1943.

[81] Mathur AB, Tonelli A, Rathke T, Hudson SM. The dissolution and characterization of Bombyx mori silk fibroin in calcium nitrate-methanol solution and the regeneration of films. Biopolymers 1997; 42(1): 61–74.

[82] Ha SW. The dissolution of Bombyx mori silk fibroin in the calcium nitrate-methanol system and wet spinning of the fibroin solution. Master Thesis at North Carolina State University 2000

[83] Nakajima A, Tanaami K. Dissolution and Chain Dimensions of Nylon6 in Metal Halide-Alcohol System. Polymer Journal 1973; 5(3): 248-254.

[84] Aoki T. Lecture Meeting, "Technique for Producing Syanthetic Leather," Japanese Soc. Mechanical Engineering, Tokyo, March 19, 1959

[85] Gotoh Y, Tsukada M, Minoura N. Effect of the chemical modification of the arginyl residue in Bombyx mori silk fibroin on the attachment and growth of fibroblast cells. J Biomed Mater Res 1998; 39: 351–357.

[86] Hermans J, McDonagh J. Fibrin: Structure and Interactions, Seminars Thromb. Heamost 1982; 8: 11–23.

[87] Santin M, LaCara F, Sada A, Peluso G. Chitosan as Matrix for Immobilization of a Thermophilic B-galactosidase Enzyme. Surface Properties of Biomaterials Oxford 1994; :25–38.

[88] Mineo HK, Garabed RB. Evaluation of a bench-top coagulation analyzer for measurement of prothrombin time, activated partial thromboplastin time, and fibrinogen concentrations in healthy dogs. AJVR 2007; 68(12): 1342-1347.

[89] Pusateri AE, McCarthy SJ, Gregory KW, Harris RA, Cardenas L, McManus AT, Goodwin CW. Effect of a chitosan-based hemostatic dressing on blood loss and survival in a model of severe venous hemorrhage and hepatic injury in swine. J Trauma 2003; 54: 177-182.

[90] Okamoto Y, Yano R, Miyatake K, Tomohiro I, Shigemasa Y, Minami S. Effects of chitin and chitosan on blood coagulaiton. Carbohydr Polym 2003; 53: 337-342.

[91] Rao SB, Sharma CP. Use of chitosan as a biomaterial: Studies on its safety and hemostatic potential. J Biomed Mater Res 1997; 34: 21-28.

[92] Lin CW, Lin JC. Characterization and blood coagulation evaluation of the water-soluble chitooligosaccharides prepared by a facile fractionation method. Biomacromol 2003; 4:1691-1697.

[93] Queiroz AAA, Ferraz HG, Abraham GA, Fernandez M, Bravo AL, Roman JS. Development of new hydroactive dressings based on chitosan membranes: Characterization and *in vivo* behavior. J Biomed Mater Res 2003; 64A: 147-154.

[94] Fischer TH, Connolly R, Thatte HS, Schwaitzberg SS. Comparison of structural and hemostatic properties of the poly-*N*-acetyl glucosamine Syvek Patch with products containing chitosan. Microsc Res Tech 2004; 63: 168-174.

[95] Ronghua H, Yumin D, Jianhong Y. Preparation and anticoagulant activity of carboxybutyrylated hydroxyethyl chitosan sulfates. Carbohydr Polym 2003; 51(4): 431-438.

[96] Tamada Y, Kulik EA, Ikada Y. Simple method for platelet counting, Biomaterials 1995; 16(3): 259-261.

[97] Prior JJ, Powers N, DeLustro F. Efficacy of a novel hemostatic agent in animal models of impaired hemostasis. J Biomed Mater Res 2000; 53(3): 252-257.

[98] Loke WK, Lau SK, Yong LL, Khor E, Sum CK. Wound dressing with sustained

antimicrobial capability. J Biomed Mater Res 2000; 53: 8-17.

[99] ICSH recommendations for measurement of erythrocyte sedimentation rate. International Council for Standardization in Haematology (Expert Panel on Blood Rheology). J Clin Pathol 1993; 46 (3): 198-203.

[100] Westergren A. Diagnostic tests: the erythrocyte sedimentation rate range and limitations of the technique. Triangle 1957; 3 (1): 20–5.

[101] Murakami Y, Yokoyama M, Nishida H, Tomizawa Y, Kurosawa H. A simple hemostasis model for the quantitative evaluation of hydrogel-based local hemostatic biomaterials on tissue surface. Colloids Surf B Biointerfaces 2008; 65(2):186-189.

[102] Asakura T, Kaplan DL. Encyclopedia of Agricultural Science, vol. 4, Academic Press, London, 1994.

[103] Takahashi Y, Gehoh M, Yuzuriha K. Structure Refinement and Diffuse Streak Scattering of Silk (*Bombyx mori*). Int J Biol Macromol 1999; 24: 127-138.

[104] Asakura T, Ashida J, Yamane T, Kameda T, Nakazawa Y, Ohgo K. A Repeated β-turn Structure in Poly(Ala-Gly) as a Model for Silk I of *Bombyx mori* Silk Fibroin Studied with 2D Spin-diffusion NMR under Off Magic Angle Spinning and Rotational Echo Double Resonance. J Mol Biol 2001; 306: 291-305.

[105] Rama Rao GV, Krug ME, Balamurugan S, Xu H, Xu Q, Lopez GP. Synthesis and characterization of silica-poly(*N*-isopropylacrylamide) hybrid membranes: switchable molecular filters. Chem Mater 2002; 14: 5075-5080.

[106] Gil ES , Frankowski DJ, Bowman MK, Gozen AO, Hudson SM, Spontak RJ. Mixed Protein Blends Composed of Gelatin and *Bombyx mori* Silk Fibroin: Effects of Solvent-Induced Crystallization and Composition. Biomacromolecules 2006; 7: 728-735.

[107] Gil ES, Frankowski DJ, Hudson SM, Spontak RJ. Silk fibroin membranes from

solvent-crystallized silk fibroin/gelatin blends: Effects of blend and solvent composition Materials Science and Engineering C 2007; 27: 426–431.

[108] Morton WE and Hearle JWS. Physical Properties of Textile Fibers. The Textile Institute, Third Edition 1993

[109] Hutton EA and Gartside J. J. Text. Inst., 1949, 40, T 161

[110] Chuang YJ, Swanson R, Raja SM, Olson ST. Heparin enhances the specificity of antithrombin for thrombin and factor Xa independent of the reactive center loop sequence. Evidence for an exosite determinant of factor Xa specificity in heparin-activated antithrombin. J Biol Chem 2001; 276 (18): 14961–14971.

[111] Bjork I, Lindahl U. Mechanism of the anticoagulant action of heparin. Mol Cell Biochem 1982; 48: 161–182.